Biophysical Journal
Article

Biophysical Society

# Stochastic dynamics and ribosome-RNAP interactions in transcription-translation coupling

Xiangting Li[1] and Tom Chou[1,2,*]
[1]Department of Computational Medicine, University of California, Los Angeles, Los Angeles, California and [2]Department of Mathematics, University of California, Los Angeles, Los Angeles, California

ABSTRACT Under certain cellular conditions, transcription and mRNA translation in prokaryotes appear to be "coupled," in which the formation of mRNA transcript and production of its associated protein are temporally correlated. Such transcription-translation coupling (TTC) has been evoked as a mechanism that speeds up the overall process, provides protection against premature termination, and/or regulates the timing of transcript and protein formation. What molecular mechanisms underlie ribosome-RNAP coupling and how they can perform these functions have not been explicitly modeled. We develop and analyze a continuous-time stochastic model that incorporates ribosome and RNAP elongation rates, initiation and termination rates, RNAP pausing, and direct ribosome and RNAP interactions (exclusion and binding). Our model predicts how *distributions* of delay times depend on these molecular features of transcription and translation. We also propose additional measures for TTC: a direct ribosome-RNAP binding probability and the fraction of time the translation-transcription process is "protected" from attack by transcription-terminating proteins. These metrics quantify different aspects of TTC and differentially depend on parameters of known molecular processes. We use our metrics to reveal how and when our model can exhibit either acceleration or deceleration of transcription, as well as protection from termination. Our detailed mechanistic model provides a basis for designing new experimental assays that can better elucidate the mechanisms of TTC.

SIGNIFICANCE Transcription-translation coupling (TTC) in prokaryotes is thought to control the timing of protein production relative to transcript formation. The marker for such coupling has typically been the measured time delay between the first completion of transcript and protein. We formulate a stochastic model for ribosome and RNAP elongation that also includes RNAP pausing and ribosome-RNAP binding. The model is able to predict how these processes control the distribution of delay times and the level of protection against premature termination. We find relative speed conditions under which ribosome-RNAP interactions can accelerate or decelerate transcription. Our analysis provides insight on the viability of potential TTC mechanisms under different conditions and suggests measurements that may be potentially informative.

## INTRODUCTION

In prokaryotic cells, transcription and translation of the same genes are sometimes "coupled" in that the first mRNA transcript is detected coincidentally with the first protein associated with that transcript. This observation suggests the proximity of the ribosome to the RNA polymerase (RNAP), as was directly observed by Miller et al. (1). These findings contributed to the idea that the ribosome and RNAP may interact directly or indirectly. Ribosome-RNAP interactions in prokaryotes are thought to maintain the processivity of RNAP by physically pushing it out of the paused, backtracking state (2). Paused RNAP has also been associated with transcriptional error correction and premature mRNA cleavage (3–6); thus, ribosome-RNAP interactions that catalyze RNAP unstalling and speeding up the overall process might do so at the expense of more errors in the transcript. Transcription-translation coupling (TTC) may also play an important role in protecting mRNA from premature transcription termination (7–9). This protection might arise from steric shielding of the elongation complex by the leading ribosome, preventing attack by Rho (9,10).

Evidence for TTC has come from two types of experiments. The first is "time-of-flight" experiments that quantify the time delay between first detection of a complete transcript and a complete protein. For example,

*Submitted June 23, 2022, and accepted for publication September 27, 2022.*
*Correspondence: tomchou@ucla.edu
Editor: Jason Kahn.
https://doi.org/10.1016/j.bpj.2022.09.041

IPTG-induced LacZ completion experiments (LacZ assays) measure the mean time of mRNA completion $\mathbb{E}[T_{\mathrm{RNAP}}]$ and the mean time of protein completion by the leading ribosome $\mathbb{E}[T_{\mathrm{rib}}]$, with the latter measured from the time of first RNAP engagement (11–13). Since the transcript length $L$ is known, the effective velocities of the RNAP and ribosome over the entire transcript can be estimated by

$$\overline{V}_{\mathrm{RNAP}} = \frac{L}{\mathbb{E}[T_{\mathrm{RNAP}}]}, \; \overline{V}_{\mathrm{rib}} = \frac{L}{\mathbb{E}[T_{\mathrm{rib}}]}. \tag{1}$$

These measurements are performed at the population level, averaging the time-dependent signal from many newly formed transcripts and corresponding proteins. Thus, the individual molecular coupling mechanisms between RNAP and ribosomes cannot be resolved by the time delay unless single-molecule time-of-flight experiments can be designed.

Another class of experiments uses a variety of in vitro and in vivo assays to probe direct and indirect molecular interactions between RNAPs and ribosomes (9,14–16). A recent structural study identified active transcription-translation complexes and confirmed an indirect molecular interaction in situ (17).

Two modes of coupling between the leading ribosome and the RNAP have been proposed. One mode of coupling occurs through a "collided expressome" in which the ribosome and RNAP are held in close proximity (9,14) by direct association, which may be mediated by entropic effects of the intervening mRNA (18). The second coupling mode occurs through a larger complex in which ribosome-RNAP interactions are mediated by the proteins NusG and NusA (15–18). There have been no reports that this mode alters elongation speeds or RNAP processivity, although both are possible. It has been shown that the NusG-coupled expressome can inhibit Rho-induced premature transcription termination (19).

Both potential coupling mechanisms require at least some moments of close proximity between the RNAP and the leading ribosome during the simultaneous transcription-translation process (see Fig. 1), followed by recruitment of NusG for the NusG-coupled expressome mechanism. The ribosome-RNAP proximity requirement can be met if the ribosome elongation speed is, on average, faster than that of the RNAP. Even if the ribosome is fast, proximity also depends on initial condition (ribosome initiation delay after RNAP initiation) and the length of the transcript $L$. Moreover, both RNAPs and ribosomes are known to experience, respectively, pausing through backtracking (6) and through "slow codons" for which the associated tRNA is scarce (20).

A number of open questions remain. In the "strong coupling" picture, the ribosome and RNAP are nearly always in contact and the ribosome is thought to maintain RNAP processivity during mRNA transcription. Without the ribosome, mRNA transcription can be particularly slow. Therefore, the ribosome elongation rate dictates the RNAP elongation rate. Administration of antibiotics to slow down translation also slowed down transcription (11).

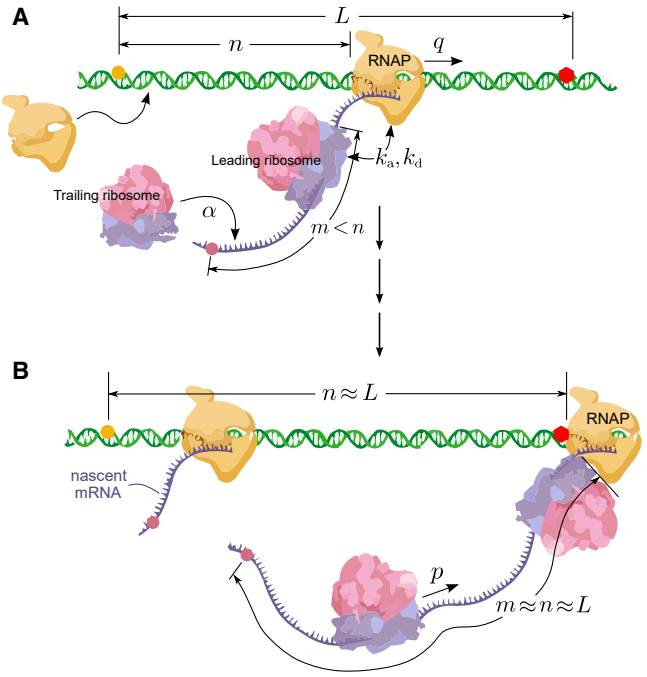


FIGURE 1 Schematic of translation of a nascent mRNA transcript (polypeptide not shown). Ribosomes translocate at rate $p$ while RNAPs elongate at rate $q$. (*A*) The transcript associated with the RNAP at position $n$ along the gene is shown with a leading ribosome at position $m$ along the mRNA. Ribosomes attach to open initiation sites at rate $\alpha$. (*B*) A nearly complete transcript is shown. If the leading ribosome has caught up to the RNAP and $m$ is close to $n$, the two may bind with rate $k_a$ to form a "coupled expressome." Ribosome-RNAP complexes can spontaneously dissociate with rate $k_d$. We assume that the leading ribosome "terminates" upon reaching the stop codon (not shown). Protein-mediated expressomes (not shown) form larger complexes that can accommodate longer mRNA segments within it.

However, other experiments have shown that the distance between the ribosome and RNAP can be large most of the time, leading to a "weak coupling" picture (21,22). The biological role of weak coupling is unclear since any shielding provided by the ribosome would be limited and ribosome and RNAP speeds could be independently modulated. Even though direct ribosome-RNAP interactions may still arise after an RNAP has stalled for a sufficiently long time, any apparent ribosome-RNAP coordination would be largely coincidental.

Besides the strong and weak coupling dichotomy, another unresolved question is whether or not TTC can slow down transcription. Traditionally, TTC has been invoked as a mechanism for maintaining RNAP processivity by rescuing RNAP from paused states. However, in vivo experiments by Kohler et al. (9) reported that, when translation is inhibited, the Δ$\alpha$CTD mutant in which RNAP *does not* associate with

ribosome exhibited faster proliferation than that of wild-type RNAP that can associate with ribosomes. Coupled transcription through ribosome-RNAP association may give rise to *slower* transcription. Although in situ cryo-EM has also shown protein-mediated complexes of ribosome and RNAP (23), additional studies should be devised to confirm and characterize ribosome-RNAP interactions in vivo. Nonetheless, our mathematical model can provide possible mechanistic insights into TTC.

To help resolve the puzzles discussed above, provide a quantitative way to explore different molecular mechanisms that may contribute to TTC, and generate predictions that can be compared with experimental observations, we formulate a stochastic model that combines a number of known molecular mechanisms from transcription, keeping track of ribosome and RNAP states and positions along the gene. While an earlier model combined transcription and translation in prokaryotes (24), it did not explicitly incorporate mechanisms of direct transcription and translation coupling and only assumed simple volume exclusion between the RNAP and the leading ribosome.

Here, we explicitly allow for RNAP pausing and formal association and dissociation of the ribosome-RNAP complex. Here, "association" will be generally used to denote specific or nonspecific, direct or indirect molecular interactions. The typical assay used to probe TTC involves measuring the time delay $\Delta T = T_{\mathrm{rib}} - T_{\mathrm{RNAP}}$ between the completion of mRNA and its associated protein. Although time delays can be used as a metric for defining TTC, absence of delay is a necessary but not sufficient condition for direct ribosome-RNAP coupling. Even a direct observation of an interacting expressome does not imply functional consequences of TTC. After formulating our model, we construct additional metrics that better define and reflect possible attributes of TTC. However, since the time delay is the most experimentally measurable quantity, we will still derive and compute the full probability density of delay times $\rho(\Delta T)$.

## MODEL AND METHODS

Based on existing structural and interaction information, we formulate a continuous-time Markov chain to model ribosome and RNAP kinetics. As shown in Fig. 1, we describe the position of the head of the leading ribosome along the nascent transcript by $m = 0, 1, \ldots, L$, where 0 denotes a ribosome-free transcript. We also track the length of the nascent mRNA transcript that has cleared the exit channel of the RNAP through the discrete variable $n = 1, 2, \ldots, L$. The positions are described in terms of triplets of nucleotides corresponding to codons, the fundamental step size during ribosome elongation.

Here, $L$ is the length of the coding region of the transcript, typically about $L \sim 300$ codons. Since we are interested in the elongation phase of coupled transcription and translation, the length $L$ is measured from the ribosome binding site immediately upstream of the start codon to the stop codon. We carefully choose the definition of $m$ and $n$ so that ribosome and RNAP sizes are irrelevant and that the difference $d \equiv n - m$ precisely describes the length of the free intervening mRNA between them. Effects of TTC on transcription termination have been previously discussed in (25,26). Therefore, $0 \leq m \leq L$, $1 \leq n \leq L$, and $n = L$ is interpreted as a completed mRNA while $m = L$ indicates a completed polypeptide. Thus triangular state-space defined by $(m, n)$ often arises in related stochastic models of interacting particles in one dimension (6,27,28). Thus far, we assumed monocistronic mRNAs. Polycistronic mRNA with multiple internal ribosome entry sites can be modeled as successive processes with shared RNAP coordinates, independent ribosomes, and $L$ being the respective cistron length.

Within each positional state $(m, n)$, the leading ribosome and RNAP can exist in different internal configurations describing their molecular states. The RNAP at site $n$ can switch between two states, a processive state and a paused state. In the processive state, the RNAP can move forward by one codon at rate $q_n$ or it can transition to a paused or "backtracking" state with stalling rate $k_-$. The RNAP elongation rate can also depend on its position $n$ through different abundances of corresponding nucleotides. For simplicity, we assume that RNAPs in the backtracking state are fixed and do not elongate ($q_n = 0$) but may transition back to the processive state with unstalling rate $k_+$. The waiting time distributions in the processive and paused states are exponential with mean $1/k_-$ and $1/k_+$, respectively. The leading ribosome at site $m$ will be assumed to always be in a processive state with forward hopping rate $p_m$ if and only if the next site $m + 1$ is empty (not occupied by the downstream RNAP). In general, the ribosome translation rate can depend on the position $m$ through the codon usage at that site.

When the distance between the leading ribosome and the RNAP is within an interaction range $\ell$, ($d \equiv n - m \leq \ell$), they may associate or "bind" with rate $k_{\mathrm{a}}$ to form a coupled expressome and dissociate with rate $k_{\mathrm{d}}$ (Eqs. 6 and 7). Note that $d \leq \ell$ simply describes proximity and not necessarily molecular coupling. In cases where ribosome-RNAP complex formation is mediated by other proteins and cofactors, such as NusG, etc., $k_{\mathrm{a}}$ would represent an effective complex formation rate that could depend on NusG availability. To enumerate coupled and paused-RNAP internal states, we define $(a, b) \in \{0, 1\}^2$ such that $a = 1$ refers to an associated, or "bound" ribosome-RNAP complex, and $b = 1$ refers to an RNAP in a backtracking, or a "paused" or "stalled" state. When $a = 0$, the ribosome is not bound to the RNAP, and when $b = 0$, the RNAP is in the processive state. The state space of our discrete stochastic model is given by $\{(m, n, a, b) : 1 \leq m \leq n \leq L, a, b \in \{0, 1\}\}$, with $\{(0, n, 0, b) : 1 \leq n \leq L, b \in \{0, 1\}\}$ representing

**TABLE 1 Model parameters**

| Parameters | Description | Typical values[a] | Refs. |
|---|---|---|---|
| $\alpha$ | translation initiation rate | $\sim 0.01 - 10.0\ s^{-1}$ | (25,30–32) [b] |
| $L$ | gene and transcript length | $L \in \mathbb{Z}^+$, $L \sim 300$ | (33) |
| $m$ | ribosome position from mRNA 5′ | $m \in \mathbb{Z}_{\geq 0}$, $0 \leq m \leq L$ | – |
| $n$ | RNAP position from mRNA 5′ | $n \in \mathbb{Z}_+$, $m \leq n \leq L$ | – |
| $p$ | free ribosome translocation rate | $\sim 15$ codons/s | (11,25,34,35) |
| $q$ | free processing RNAP transcription rate | $\sim 30$ codons/s | (11–13,36) [c] |
| $k_-$ | processive RNAP $\rightarrow$ paused RNAP rate | $\sim 0.4\ s^{-1}$ | (37) [d] |
| $k_+$ | paused RNAP $\rightarrow$ processive RNAP rate | $\sim 0.3\ s^{-1}$ | (37) |
| $k_+^*$ | paused RNAP $\rightarrow$ processive RNAP rate (pushed) | $k_+^* = k_+ \exp(E_+), E_+ \geq 0$ | estimated |
| $k_a, k_d$ | ribosome-RNAP association, dissociation rates | $k_d = k_a e^{-E_a}$, $E_a \sim 3 - 7$ | (14) |
| $\ell$ | maximum mRNA length in bound complex | $\sim 4 - 6$ codons | (29) |

[a]The unit of length assumed throughout the paper will be nucleotide triplets (codons).
[b]Translation initiation is highly variable. In accordance with LacZ completion assays (25,30), we initially set $\alpha = 1/s$ in our simulations and later discuss the effects of varying translation initiation rates.
[c]Typical noninteracting RNAP transcription rates are $\overline{q} \equiv q k_+/(k_- + k_+) \sim 15$ codons/s. Since typically $k_+/(k_+ + k_-) \sim 1/2$, we use typical values $q \sim 30$ codons/s for the unimpeded transcription rate of processing RNAP.
[d]The pausing probability along an RNAP trajectory has been measured as $\sim 0.87$ per 100 nucleotides. By using the estimated mean RNAP velocity of $\sim 15$ codons/s, we convert this probability to a pausing rate $k_- \approx 0.4$/s.

ribosome-free configurations. By appropriately choosing $\ell$, $k_a$, and $k_d$, our model can effectively describe both the collided expressome and the NusG-mediated expressome. Experimentally, the collided expressome is typically observed in a stalled configuration (9,17,18,29). This observation is consistent with a small $k_a$ and a large $k_d$, which suggests that the coupled, processive state $a$ is transient. We will define $\log(k_a/k_d) \equiv E_a$ which is not restricted to positive values.

Other than steric exclusion (which constrains $m \leq n$) and ribosome-RNAP association and dissociation, we incorporate a contact-based RNAP "pushing" mechanism. The processing ribosome can directly push (powerstroke) against a stalled RNAP and/or reduce the entropy of a backtracking RNAP to bias it toward a processive state. A similar mechanism arises in RNAP-RNAP interactions, as discussed in (6). To quantify this pushing mechanism, we simply modify the paused-to-processive RNAP ($b = 1 \rightarrow b = 0$) transition rate from $k_+$ to $k_+^* \equiv k_+ e^{E_+} > k_+$ whenever the ribosome abuts the RNAP ($d \equiv n - m = 0$). The enhanced rate arises from a reduction $E_+$ in the total transition free energy barrier provided by the adjacent ribosome. Typical model parameters relevant to prokaryotic transcription and translation are listed in Table 1.

The length $\ell$ may influence direct molecular coupling and stochastic dynamics of transcription. In vitro studies of ribosome and RNAP structure provide constraints on the configuration space accessible to coupled expressomes. Wang et al. (29) and Webster et al. (18) found that collided expressomes are stable only when the spacer mRNA between the ribosome and the RNAP is $\sim 12 - 24$ nucleotides ($\sim 4 - 8$ codons). Because the intervening mRNA must be at least 12 nucleotides to extend beyond the RNA exit channel of the RNAP, the free intervening RNA within an intact collided expressome can vary between 0 and 12 nucleotides. In contrast, the NusG-mediated expressome can accommodate $\sim 24 - 30$ free mRNA nucleotides. RNA looping might allow for even longer spacer mRNA, but there has so far been no in vivo evidence that collided expressomes exist with mRNA loops.

Since mRNA is flexible, we can also assume that $k_d$ is constant for $d \equiv n - m \leq \ell$. The association rate $k_a$ may be dependent on the distance $d = n - m$ between the ribosome and the RNAP; for example, a distance-dependent association rate might take the form $k_a(n - m) \approx k_a(\ell)[(\ell + \xi)/(n - m + \xi)]^3$, where $[(n - m) + \xi]^{-3}$ represents the effective volume fraction of the leading ribosome and $\xi$ is the configuration flexibility of ribosome-RNAP binding when they are close. If we adopt such a distance-dependent $k_a$, we would also have to let the ratio $p/q$ be dependent on $(n - m)$ in order to conserve free energy during approach and binding steps. To simplify matters, we will assume that $\xi \gg \ell$ and take $k_a$ to be a constant for $d \equiv n - m \leq \ell$ and zero for $d \equiv n - m > \ell$.

The overall kinetics of the internal states pictured in the insets of Fig. 2 can be explicitly summarized by considering the intervening mRNA length $d = n - m$ between RNAP and the ribosome. Fig. S1 in Appendix S1 explicitly depicts the transitions for different $d$. Since, in our model, the maximum length of mRNA that can fit within the complex is $\ell$, a processing ribosome-bound RNAP at $n = m + \ell$ cannot advance to lengthen the already compressed transcript (see Fig. 2 *E*). The only way a coupled state $a = 1$ with $d = \ell$ can reach any state where $d > \ell$ is for the ribosome and RNAP to first dissociate (we assume dissociation rates in all $d = n - m$ states remain constant at $k_d$). Molecular coupling effectively slows down transcription by preventing RNAP elongation in the $a = 1$, $d = \ell$ state. Such ribosome-mediated slowing down of transcription has been proposed in previous studies (2,9).

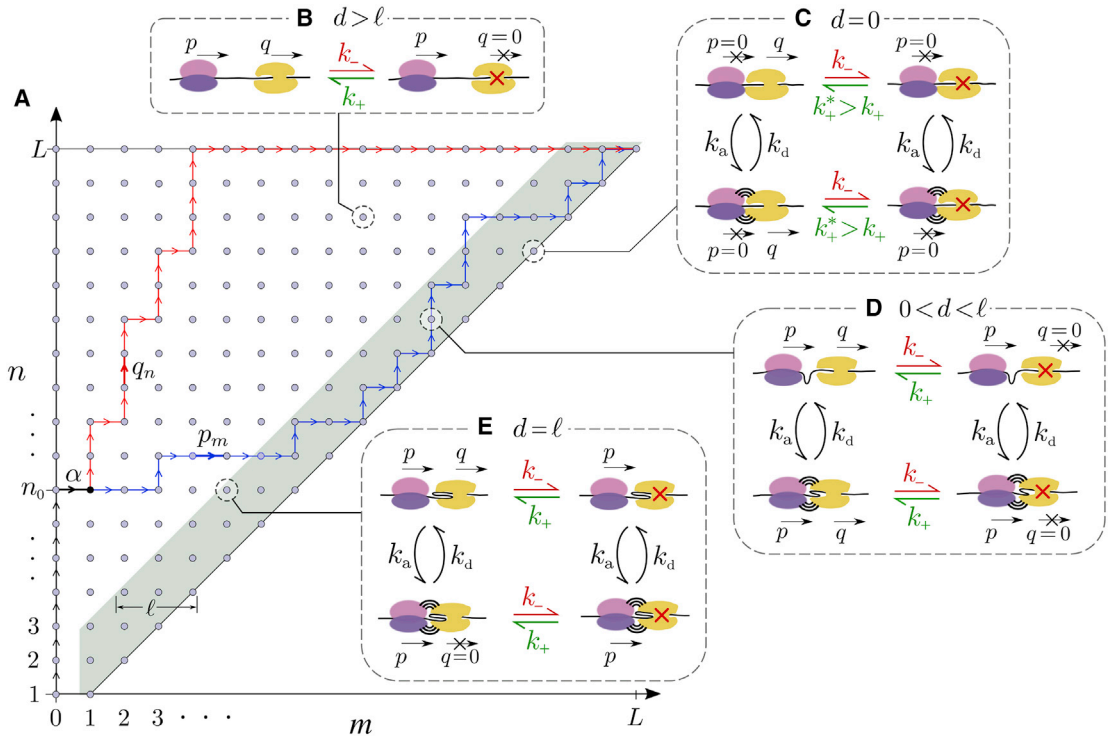


FIGURE 2 (*A*) State space of the stochastic model defined in terms of the leading ribosome and RNAP positions $(m, n)$. The initial time $t = 0$ is defined as the time RNAP first produces a ribosome initiation site, starting the system in $(m = 0, n = 1)$. For $t > 0$, as the RNAP is elongating, the first ribosome binds at rate $\alpha$. Here, a ribosome binds after the RNAP first reaches position $n = n_0$. Red and blue trajectories indicate scenarios in which the RNAP is relatively fast and slow, respectively. Within each position $(m, n)$ exist internal molecular microstates. (*B*) In the "interior" states $n - m > \ell$ ($\ell = 2$ in this example), the ribosome and RNAP are too distant to be bound, and only stalled and processing RNAP states arise, with transition rates $k_\pm$ between them. (*C*) When $d = n - m = 0$, the ribosome and RNAP are adjacent without any intervening mRNA, allowing them to associate with rate $k_a$. The RNAP can be in either stalled or processive states. In the stalled state, whether associated or not, the adjacent volume-excluding ribosome entropically "pushes" the stalled RNAP, catalyzing its transition to a processive state so that $k_+^* > k_+$. (*D*) When $0 < n - m < \ell$, the ribosome and the RNAP are close enough to bind with rate $k_a$. Here, the intervening mRNA dissipates the entropic pushing (so that the stalled RNAP $\rightarrow$ processing RNAP transition rate is $k_+$) and also allows an RNAP in the processive state to elongate with rate $q$, regardless of whether it is bound to the ribosome. (*E*) Only when the ribosome and the RNAP are separated by $d = \ell$ is a bound RNAP prevented from processing as this would reel in more mRNA than can be fit inside the complex, either a collided or NusG-mediated expressome. Molecular binding prevents complexed ribosome and RNAP to be separated by more than $\ell$ mRNA codons.

We now list all allowed transitions in the $\omega := \{m, n, a, b\}$ state space of our continuous-time stochastic Markov model. The probability that an allowable transition from state $\omega$ to state $\omega'$ occurs in time increment d$t$ is $r(\omega'|\omega)$d$t$, where the complete set of rates is given by

$$r(1, n, a, b \mid 0, n, a, b) = \alpha, \qquad 1 \le n \le L, \tag{2}$$

$$r(m+1, n, a, b \mid m, n, a, b) = p_m, \quad 1 \le m \le n-1, \tag{3}$$

$$r(m, n+1, 0, 0 \mid m, n, 0, 0) = q_n, \quad m \le n \le L-1, \tag{4}$$

$$r(m, n+1, 1, 0 \mid m, n, 1, 0) = q_n, \quad 0 \le d \le \ell - 1, \tag{5}$$

$$r(m, n, 1, b \mid m, n, 0, b) = k_a, \qquad 0 \le d \le \ell, \tag{6}$$

$$r(m, n, 0, b \mid m, n, 1, b) = k_d, \tag{7}$$

$$r(m, n, a, 1 \mid m, n, a, 0) = k_-, \tag{8}$$

$$r(m, n, 0, 0 \mid m, n, 0, 1) = k_+, \tag{9}$$

$$r(m, n, 1, 0 \mid m, n, 1, 1) = k_+^*, \qquad a = 1,\ m = n. \tag{10}$$

Using these rules, we performed event-based stochastic simulations (38,39) of the model as detailed in Appendix S1 of the supporting material. For completeness, the master equation associated with our model is also formally given in Appendix S2.

## Construction of time-delay distribution

Our stochastic molecular model allows for the explicit calculation of the probability density $\rho(\Delta T)$ of time delay $\Delta T = T_{\text{rib}} - T_{\text{RNAP}}$ between mRNA and polypeptide completion. To find $\rho(\Delta T)$, we first find the distribution of ribosome positions $m(T_i)$ at the moment $T_i \equiv T(n = i)$ the RNAP first reaches site $i$. $T_L \equiv T_{\text{RNAP}}$ denotes the

instant the mRNA is completed. The initial value $m(T_1) = 0$ is known because, immediately after initiation of RNAP at site $n = 1$, the ribosome is not yet present but is trying to bind at a rate of $\alpha$. As detailed in Appendix S3, we can iteratively find the distribution of $m(T_{i+1})$ given that of $m(T_i)$. By the same method, the distribution of association values $a(T_{\mathrm{RNAP}})$ at the instant of RNAP completion can be computed. After constructing the probability distribution $\mathbb{P}(m,a,b \mid t = T_{\mathrm{RNAP}})$, we evolve it to find the distribution of the additional amount of time $\Delta T = T_{\mathrm{rib}} - T_{\mathrm{RNAP}}$ required for $m$ to first reach $L$.

Although we are able to construct the whole distribution of delay times that might provide a more resolved metric, especially if single-molecule or single-cell assays can be developed, a short time delay is a necessary but not sufficient condition for TTC. To provide direct information on molecular ribosome-RNAP interactions, we construct additional metrics.

## Analytic approximation

Although our stochastic model contains a complex state space with many parameters, simple physical limits are immediately apparent. If the free ribosome translocation rate $p$ is much greater than the free RNAP transcription rate $q$ and $\alpha \gg L/\overline{q}$, the ribosome, for much of the time, abuts the RNAP, inducing it to transcribe at an average rate $qk_+^*/(k_+^* + k_-) \equiv \overline{q}^*$. Here, we predict an expected delay $\mathbb{E}[\Delta T] \approx 0$, $C \approx k_{\mathrm{a}}/(k_{\mathrm{a}} + k_{\mathrm{d}})$, and $F_T \approx 1$. If the ribosome is slow and $p \ll \overline{q}$, the ribosome and RNAP are nearly always free, $\Delta\mathbb{E}[T] \approx 1/\alpha + L(1/p - 1/\overline{q})$, $C \approx 0$, and $F_T \approx 0$. However, when $p$ is intermediate, more intricate kinetics can arise, including tethered elongation and transcription slowdown.

To gain insight into this intermediate case, we first assume the large system limit $L \to \infty$ and divide the states into those with $d > \ell$ and those with $d \leq \ell$. Within each metastate, the behavior of the ribosome and RNAP is relatively homogeneous. States with $d > \ell$ are completely decoupled, while the proximal states $d \leq \ell$ can include associated $(a = 1)$ or unassociated $(a = 0)$ ribosome/RNAP substates.

To characterize the transition between the two metastates, we define the mean dwell time in metastate $d > \ell$ by $T_0$ and the mean dwell time in the metastate $d \leq \ell$ by $T_1$. The variability in the $d > \ell$ state dwell time arises mainly from RNAP stalling and unstalling. When translation is slow, the RNAP may undergo multiple stalling-unstalling cycles before leaving the $d > \ell$ metastate. For faster translation, one stalling event will typically be enough to leave the $d > \ell$ metastate. Let $P_0 = p/[p + (q-p)k_+/k_-]$ be the probability of leaving $d > \ell$ following one RNAP stalling event. With details provided in Appendix S4 of the supporting material, we find analytic approximations to $T_0$ and $T_1$ in the $q > p > \overline{q}$ and small $\ell$ limit:

$$T_0 \approx \frac{q}{pk_-} + \left(\frac{1}{k_-} + \frac{1}{k_+}\right)\left[\frac{(q-p)k_+}{pk_-} + \frac{(1-P_0)(q-p)/k_-}{p/k_+ - (q-p)/k_-}\right], \tag{11}$$

$$T_1 \approx \frac{k_{\mathrm{a}} + k_{\mathrm{d}}}{k_{\mathrm{d}}}\left(1 + \frac{k_-}{k_+^*} + \frac{k_-\ell}{p}\right)\left(\frac{1}{p} + \frac{1}{q}\right)\left(\frac{p}{q}\right)^{\ell}\sum_{j=1}^{\ell} j\left(\frac{q}{p}\right)^{j}. \tag{12}$$

As $p \downarrow \overline{q}$, the ribosome and RNAP are less likely to be proximal and $T_0 \to +\infty$. Once $p \leq \overline{q}$, the RNAP and the ribosome remain separated. On the other hand, as $p \uparrow q$, $1 - P_0 \to 1$, $T_0 \to 1/k_-$, and $T_1$ is always monotonically increasing with $p$. Kinetics between these two metastates qualitatively capture the behavior of the model in the translation-invariant, infinite length limit. The approximations, $T_0$ and $T_1$ will used in some of our subsequent results.

## Metrics of TTC

We now define additional metrics that help characterize TTC. To more explicitly quantify direct *molecular* coupling, we define the *coupling coefficient* $C$ by

$$C \equiv \mathbb{P}(a = 1 \mid t = T_{\mathrm{RNAP}}), \tag{13}$$

the probability that the ribosome is associated with the RNAP $(a = 1)$ at the moment the mRNA transcript is completed. The coupling parameter $C$ provides a more direct measure of molecular coupling and further resolves configurations that have short or negligible delays. While delay time distributions do not directly quantify ribosome-RNAP contact, the coupling coefficient $C$ does not directly probe the trajectories or history of ribosome-RNAP dynamics.

To also characterize the history of ribosome-RNAP interactions, we quantify TTC by the fraction of time $F_T$ that the ribosome "protects" the RNAP across the entire transcription process. There are different ways of defining how the transcript is protected. While both modes of TTC are proposed to shield the mRNA from premature termination, neither has been directly observed in vivo. We assume that a termination protein has size $\sim \ell_{\mathrm{p}}$ and that, if the ribosome and RNAP are closer than $\ell_{\mathrm{p}}$, the termination factor is excluded. Thus, we define the protected time as the total time that $d < \ell_{\mathrm{p}}$ codons, divided by the time to complete transcription:

$$F_T = \frac{\| \{t : (n_t - m_t < \ell_{\mathrm{p}})\} \|}{T_{\mathrm{RNAP}}}. \tag{14}$$

Since the transcription-termination protein Rho has an mRNA footprint of about 80 nt, $\ell_{\mathrm{p}} \approx 27$ codons (40). A high $F_T$ reflects transcription that has been protected against exposure to Rho-mediated termination. The fraction of transcription events that is prematurely

terminated is then proportional to $1 - F_T$. Exploration of this fraction under different conditions might be a way to experimentally estimate $F_T$.

Using these metrics, including the effective velocities $\overline{V}_{\text{rib}}$ and $\overline{V}_{\text{RNAP}}$, we will explore properties and predictions of our model.

## RESULTS AND DISCUSSION

Here, we present analyses of solutions to our model obtained from numerical recursion and Gillespie-type kinetic Monte Carlo simulations detailed in Appendices S1, S2, and S3 of the supporting material. Predictions derived from using different parameter sets are compared, and mechanistic interpretations are provided.

### Comparison of TTC metrics

We evaluate our stochastic model to provide quantitative predictions for the coupling indices, $\rho(\Delta T)$, $C$, and $\mathbb{E}[F_T]$. The results are summarized in Fig. 3.

#### *Limitations of mean delay times*

Fig. 3 *A* shows delay-time distributions for various parameter sets and reveals subtle differences in the kinetic consequences of coupling. Without molecular coupling ($k_a = 0$), the distribution has a single peak around the mean delay time. With molecular coupling, the distribution can exhibit two peaks with one at $\Delta T = 0$. This short-time peak reflects trajectories that terminate as a bound ribosome-RNAP complex. These finer structures in $\rho(\Delta T)$ cannot be resolved by evaluating only the mean delay time. Fig. 3 *B* plots the mean delay $\mathbb{E}[\Delta T]$ as a function of $p$ and $q$. For our chosen parameters, in particular $k_a = 100$/s and $k_d = k_a e^{-3}$, we see that $\mathbb{E}[\Delta T]$ is rather featureless, with a significant delay arising only for small $p$. Thus, the mean delay time provides little information about the details of TTC.

#### *Coupling coefficient*

The dimensionless ratio $p/\overline{q}$ is a key indicator of the overall level of coupling possible. If $p/\overline{q} > 1$, the speed of the ribosome exceeds the average speed of the RNAP, allowing them to approach each other and potentially form a coupled expressome. If $p/\overline{q} < 1$, the ribosome speed is slower than the average RNAP speed and the system can at most be only transiently coupled. It turns out that the coupling coefficient $C$ is mostly determined by $p/\overline{q}$ alone, particularly if the effects of translation initiation vanishes for large $L$ (see "effects of translation initiation rates" section later). Essentially, the transition to a coupled system (large $C$) is predicted when $p/\overline{q} \gtrsim 1$. In Fig. 3 *C*, we find the values of $C$ for multiple values of $p$ and $q$ (each dot corresponds to each $(p, q)$ pair), and plot them as a function of $p/\overline{q}$, with $k_+/(k_+ + k_-) \approx 0.43$. The mean values of $C$ as a function of $p$ and $q$ are plotted in Fig. 3 *D* and are qualitatively distinct from the mean times shown in (*B*). Given Eqs. 11 and 12, the steady-state coupling coefficient $C$ for $L \to \infty$ can be approximated as

$$C \approx \frac{k_a}{k_a + k_d} \frac{T_1}{T_1 + T_0}, \tag{15}$$

which qualitatively agrees with numerical results as shown in Fig. 3 *C*.

#### *Fraction of time protected*

Each point in Fig. 3 *E* indicates the mean value $F_T$, $\mathbb{E}[F_T]$, for different values of $p$ and $q$, arranged along values of $p/\overline{q}$. Each value $\mathbb{E}[F_T(p,q)]$ was computed by averaging protected-time fractions $F_T$ (Eq. 14) from 1000 simulated trajectories. As expected, $\mathbb{E}[F_T(p,q)]$ increases with ribosome translation rate $p$ until saturation to above $\mathbb{E}[F_T] \gtrsim 0.9$ for $p \gtrsim 22$ codons/s.

Comparing $C$ and $\mathbb{E}[F_T]$ from Fig. 3 *D* and *F* we find that $C$ and $\mathbb{E}[F_T]$ are qualitatively similar across various values of $p$ and $q$, although in general we find $\mathbb{E}[F_T] \gtrsim C$. The transition from low to high values occurs at lower values of $p$ for $\mathbb{E}[F_T]$ since the condition for protection ($d \le \ell_p$) is not as stringent as that for $C = 1$ ($d \le \ell$ and binding). Thus, there can be value of $(p, q)$ for which $C(p,q)$ is small but $\mathbb{E}[F_T(p,q)]$ is close to one.

The similarity between $\mathbb{E}[F_T]$ and $C$ is restricted to the dependence on $p$ and $q$. The coupling and the protection time fraction may respond to changes in other parameters in drastically different ways. For example, $C$ is nonzero only if molecular binding is present, rendering it sensitive to $k_a$, $k_d$. However, $F_T$ directly measures the dynamics of TTC and does not depend on actual molecular coupling, so it will be relatively insensitive to $k_a$, $k_d$, particularly when $p$ is large. Thus, $F_T$ may be a better index if we wish to quantify functional consequences of TTC. The standard deviation of the simulated $F_T$ values is large and approximately $\sqrt{\mathbb{E}[F_T](1 - \mathbb{E}[F_T])}$ (shown in Appendix S5 of the supporting material), limiting the suitability of the mean protected-time fraction as a robust metric.

As with the coupling coefficient $C$, $F_T$ can be estimated under our heuristic approximations:

$$F_T \approx \frac{T_1}{T_1 + T_0} + \frac{\frac{q}{pk_-} + \left(\frac{1}{k_-} + \frac{1}{k_+}\right)\frac{(q-p)k_+}{pk_-}}{T_0 + T_1}\left(1 - e^{-\frac{k_-}{q-p}(\ell_p - \ell)}\right). \tag{16}$$

From Eq. 16, we see that $F_T$ is comprised of two terms, the protection provided by coupling $\frac{T_1}{T_1+T_0} \approx \frac{k_a+k_d}{k_a} C$, and the protection provided by ribosome elongation when $d > \ell$. Although Eq. 16 is valid mainly

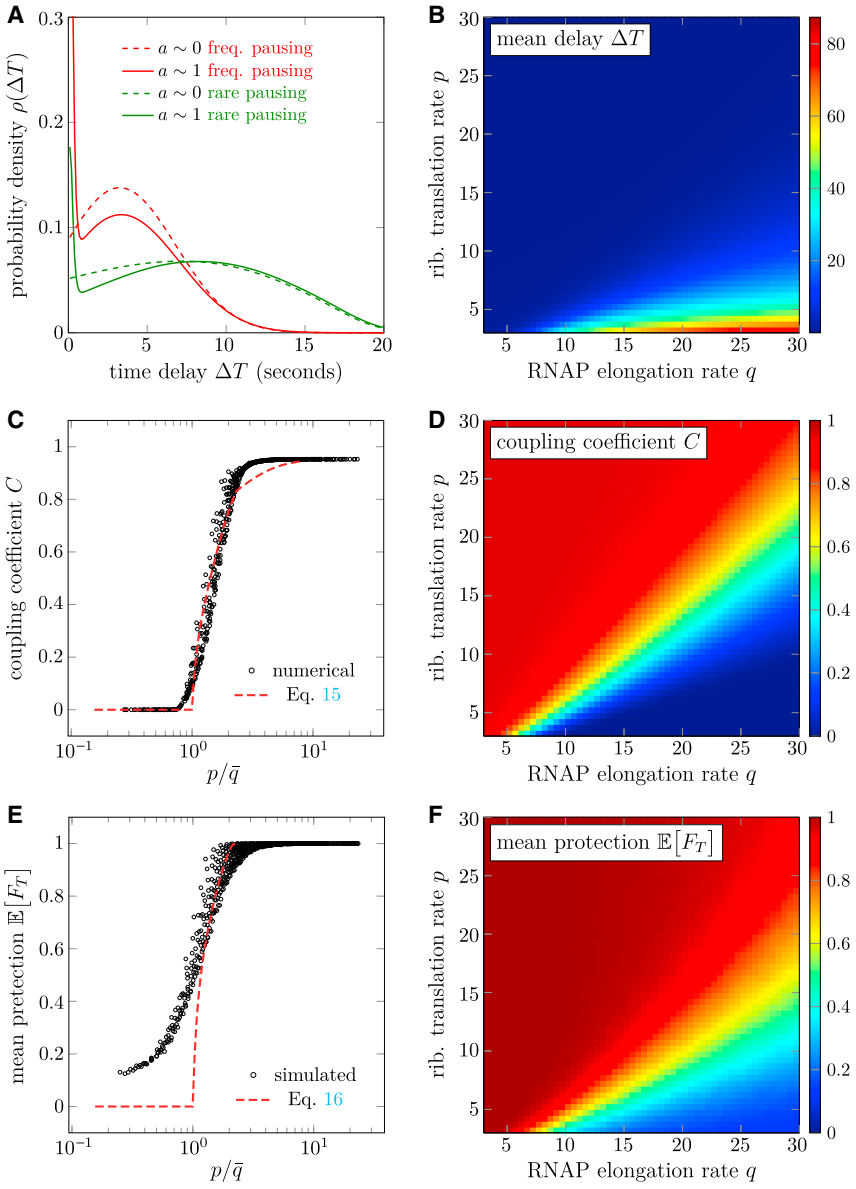


FIGURE 3 Comparison of different TTC indices. Common parameters for all these plots are $\alpha = 1$/s, $E_+ = 2$, $E_a = 3$, $k_d = k_a e^{-E_a}$, $\ell = 4$, $L = 335$, and $k_a = 100$/s, unless stated otherwise. (*A*) The delay-time density $\rho(\Delta T)$ plotted for $p = 12$ codons/s and $q = 30$ codons/s. Densities for $k_+ = 0.4$/s, $k_- = 0.3$/s (rarely pausing RNAPs, *green curves*), and $k_+ = 4.0$/s, $k_- = 3.0$/s (frequently pausing RNAPs, *red curves*) are shown. Within these cases, strong-binding ($a \sim 1$, $k_a = 100$/s, $k_d = k_a e^{-3}$) and no-binding ($a = 0$, $k_a = 0$) subcases are indicated by solid and dashed curves, respectively. (*B*) Mean delay $\mathbb{E}[\Delta T]$ as a function of $p$ and $q$. (*C*) The direct coupling coefficient $C$ as a function of the relative velocity $p/\overline{q}$. Each point represents $C$ evaluated at specific values of $(p,q)$, each chosen from all integers between 3 and 27 codons/s. The dashed curve represents the analytic approximation given by Eq. 15. (*D*) Heatmap of $C(p,q)$. (*E*) Values of $\mathbb{E}[F_T]$, each derived from 1000 kinetic Monte-Carlo (kMC) trajectories, plotted against $p/\overline{q}$. The analytic approximation given by Eq. 16 is shown by the dashed curve. (*F*) The heatmap of $\mathbb{E}[F_T(p,q)]$.

for positive $E_a$ and $\ell_p > \ell$, the protection from physical proximity exists even if molecular association is completely absent. This formula confirms our observation that $\mathbb{E}[F_T] \gtrsim C$.

## Binding-induced slowdown

We now use our model to reveal the major factors contributing to TTC-induced slowdown of transcription and discuss limits this slowdown.

### *Unstalling rate $k_+^*$ dictates ribosome efficiency*

The principal factor that influences the overall velocity $\overline{V}$ of a coupled expressome is the interplay between two antagonistic mechanisms: ribosome-mediated dislodging of an adjacent stalled RNAP and bound-ribosome deceleration of the RNAP. When the reduction in activation free energy of unstalling, $E_+ = \log(k_+^*/k_+)$, is large, the ribosome is less likely to be impeded by a stalled RNAP. Fig. 4 *A* plots the effective velocities $\overline{V}_{rib}$ and $\overline{V}_{RNAP}$ as a function of $E_+$ and illustrates the increases in overall speed when the ribosome is more effective at dislodging a stalled RNAP (higher $E_+$).

The decrease in the velocity of a coupled processing RNAP is primarily determined by the ribosome translation speed $p$. For different values of $E_+ = \log(k_+^*/k_+)$, the dependence of $\overline{V}_{RNAP}$ on $p$ can be quite different, as is shown in Fig. 4 *B*. For large $E_+$, when the ribosome efficiently pushes stalled RNAPs, increasing $p$ allows the ribosome to more frequently abut the RNAP and dislodge

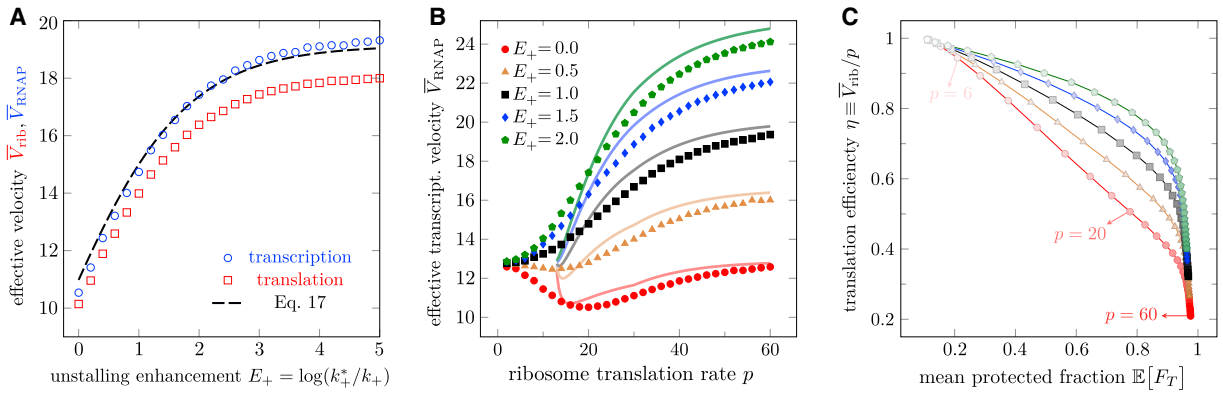


FIGURE 4 Slowdown induced by molecular coupling. The common parameters used are the same as those in Fig. 3. (*A*) Effective velocities as a function activation energy reduction $E_+ = \log(k_+^*/k_+)$ in ribosome-induced RNAP unstalling, $p = 20$ codons/s and $q = 30$ codons/s. (*B*) Effective velocity of RNAP as a function of the free ribosome translation rate $p$. (*C*) The trade-off between translation efficiency and mean fraction of time protected $\mathbb{E}[F_T]$. The efficiency $\eta \equiv \overline{V}_{\rm rib}/p$ is defined by the ratio of the mean ribosome speed to the translation rate of an isolated ribosome. In (*B*) and (*C*), $q = 30$ codons/s. The variances (not shown) for the plotted quantities are large, typically overlapping the mean-value curves in (*A* and *B*). The dashed curve in (*A*) and solid curves in (*B*) are the analytical predictions of the effective velocities using Eq. 17. To see this figure in color, go online.

it, leading to faster overall transcription. However, for inefficient unstalling (small $E_+$), we see that faster ribosomes can *decrease* $\overline{V}_{\rm RNAP}$. This feature arises because for inefficient unstalling, a larger $p$ increases the fraction of time the ribosome and RNAP are bound ($a = 1$), allowing a binding-induced slowdown to arise more often. Besides $E_+$, the emergence of a decreasing transcription velocity $\overline{V}_{\rm RNAP}$ with increasing ribosome translation rate $p$ depends intricately on factors, such as $\ell$, $k_\pm$, $k_{\rm a}, k_{\rm d}$, and arises only if $k_{\rm a}/k_{\rm d}$ is sufficiently large and $\ell$ is not too large.

Although the decrease in $\overline{V}_{\rm RNAP}$ is not large, it certainly suggests that increasing $p$ under small $E_+ \leq 0.5$ is not advantageous. This observation motivates us to define a translation efficiency as the ratio of the effective ribosome speed $\overline{V}_{\rm rib}$ to its unimpeded translation speed $p$: $\eta \equiv \overline{V}_{\rm rib}/p$. The loss $1 - \eta$ measures how much a ribosome is impeded due to its interactions with the RNAP. As $p$ is increased, we find trajectories that display a trade-off between translation efficiency and protected time. Higher $p$ leads to more proximal ribosomes and protected RNAP at the expense of translation efficiency $\eta$. Fig. 4 *C* shows that the decrease in unstalling activation energy $E_+$ affects this level of trade-off. For large $E_+$, increasing $p$ can speed up ribosomes beyond the velocity determined by $\overline{q}$ so that $\eta$ decreases more slowly than $\sim 1/p$. At the same time, the system is only slightly less coupled, leading to a subtle decrease in $\mathbb{E}[F_T]$. In the end, larger $E_+$ leads to a higher $\eta$ versus $\mathbb{E}[F_T]$ curve.

Low $\eta$ values are likely selected against since a cell would be expending more resources than necessary to maintain high levels of tRNA and other translation factors. A potentially optimal setting may be to maintain $p \simeq \overline{q}$, which is the minimally sufficient velocity to keep the RNAP protected. This intermediate choice of $p$ for the ribosome may explain the recent observations that slower ribosomes did not appreciably slow down transcription (22) or prevent folding of specific mRNA segments (21).

When $p > \overline{q}$ and $L \to \infty$, the ribosome and the RNAP intermittently close on each other and share a common effective velocity. In states $d > \ell$, the velocity $v_0 = \min\{p, q\}$ is determined by the slower of the ribosome or the processive RNAP. While the system is in states $d \leq \ell$, its velocity is given by $v_1 \approx q\left[\frac{(q/p)^\ell - 1}{(q/p)^{\ell+1} - 1}\right] \frac{k_+^*}{k_+^* + k_-}$, as detailed in Appendix S4. Finally, the overall effective velocity is estimated by

$$\overline{V} \approx \frac{T_0}{T_0 + T_1} v_0 + \frac{T_1}{T_0 + T_1} v_1. \tag{17}$$

Eq. 17 agrees qualitatively well with simulation and reproduces the slowdown, as shown in Fig. 4 *A* and *B*.

### *Limits of binding-induced slowdown*

When $\overline{q} < p < q$ and $L \to \infty$, we explore the lower bound for the effective velocity of RNAP by examining $v_1$. For sufficiently large $\ell \geq 1$ and $q/p$, the term $\left[\frac{(q/p)^\ell - 1}{(q/p)^{\ell+1} - 1}\right]$ is approximately $p/q$, and lower bounds for $\overline{V}_{\rm RNAP}(a = 1)$ are

$$\overline{V}_{\rm RNAP} \geq \frac{p k_+}{k_+ + k_-} \geq q\left(\frac{k_+}{k_+ + k_-}\right)^2. \tag{18}$$

The first equality holds when $k_+^* = k_+$, and the second equality holds when $p = \overline{q}$. We conclude that the maximum slowdown induced by binding is essentially limited by the slowdown of RNAP due to transcriptional road blocks. The latter plays a fundamental role in the significantly slower rate of mRNA transcription $\sim 45$ nt/s relative to rRNA transcription $\sim 90$ nt/s.

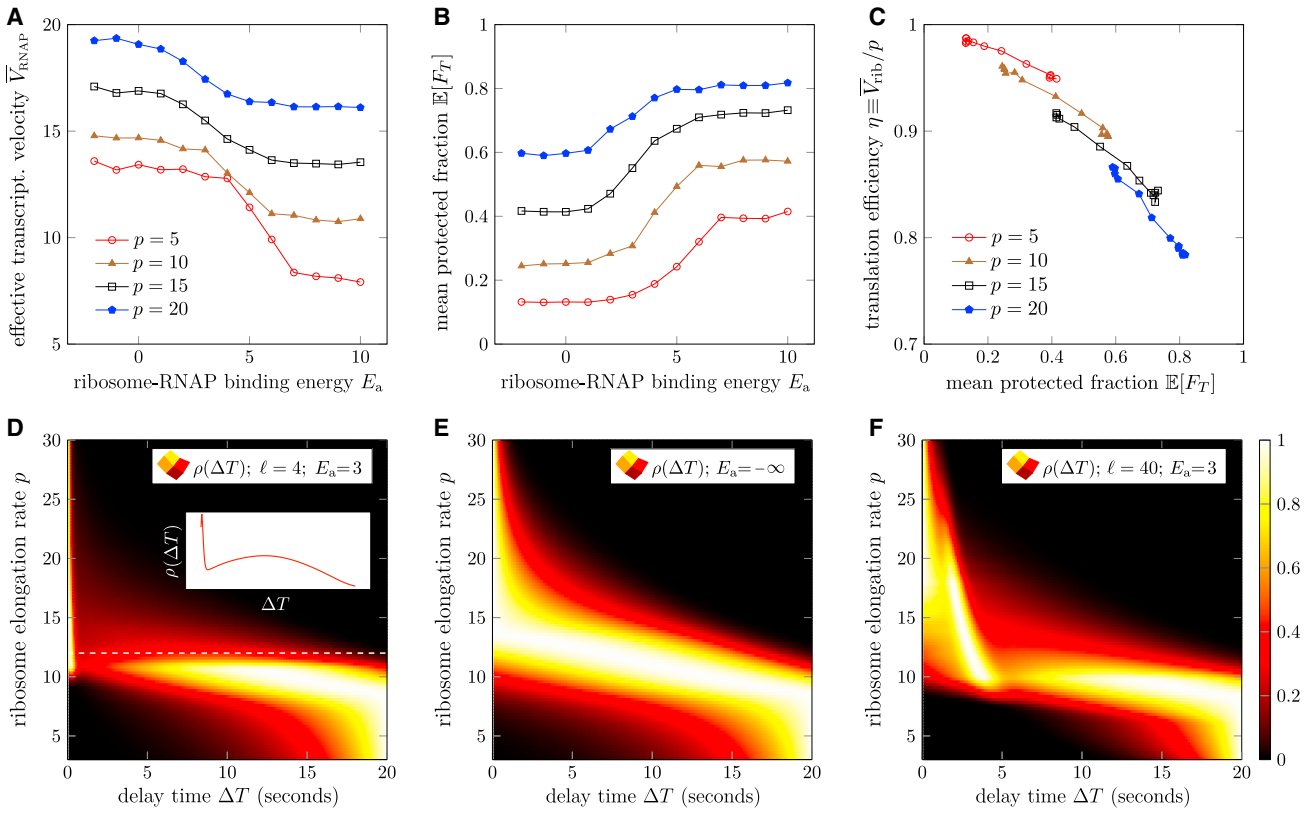


FIGURE 5 Effects of molecular coupling. For those parameters not varied, we use the same values used to generate Figs. 3 and 4. (*A*) For $\ell = 4$, the effective transcription velocity $\overline{V}_{\rm RNAP}$ as a function of binding-energy depth between the ribosome and RNAP $E_a$. (*B*) Mean protected-time fraction $\mathbb{E}[F_T]$ as a function of binding energy depth $E_a$ ($\ell = 4$). (*C*) The trade-off between efficiency and protection for $\ell = 4$. (*D*) Rescaled heatmap of the delay-time distribution $\rho(\Delta T)$ as a function of ribosome translocation rate $p$. The brightness indicates the relative probability, and the inset shows the probability distribution at $p = 12$ codons/s indicated by the dashed white line. Here, the binding energy $E_a = 3$ and $\ell = 4$. For $p \approx 9$ codons/s, $\rho(\Delta T)$ is bimodal in $\Delta T$. (*E*) Delay-time distribution in the absence of ribosome-RNAP binding ($k_a = 0$). Here, the $\ell$ dependence disappears and $\rho(\Delta T)$ is mono-modal. (*F*) Delay-time distribution for $\ell = 40$ and $E_a = 3$. Bimodality arises in more than one regime of $p$. To see this figure in color, go online.

## Testing the molecular coupling hypothesis

It is informative to use our proposed indices to compare scenarios that predict molecular coupling to those that do not. We now vary the binding energy $E_a$ for different velocity ratios $p/\overline{q}$. For $\ell = 4$, Fig. 5 *A* shows $\overline{V}_{\rm RNAP}$ as a function of $E_a$ for various values of $p$. Although higher $p$ leads to increased $\overline{V}_{\rm RNAP}$, for each value of $p$, increasing the binding energy increases coupling and leads to RNAP slowdown. Since the most significant slowdown arises when translation is slow, association-induced slowdown is indicative of strong coupling. Both $p$ and $E_a$ increase $\mathbb{E}[F_T]$, as shown in Fig. 5 *B*. The variation in $\overline{V}_{\rm RNAP}$ and $\mathbb{E}[F_T]$ with $E_a$ also suggests that, within the context of our model, one can use experimental measurements of these indices to estimate $E_a$. As $E_a$ is tuned in our model we also predict a trade-off between ribosome efficiency and protection, as shown in Fig. 5 *A*. Since our analytic approximation is most accurate in the $p \geq \overline{q}$, $L \to \infty$ regime, deviations in $\overline{V}_{\rm RNAP}$ and $\mathbb{E}[F_T]$ are mainly due to finite $L$ effects when $p < \overline{q}$; thus, we forgo plotting our analytic approximations in Fig. 5 *A–C*. In Appendix S6, we provide additional simulation results that confirm the $\ell$ dependence in Eq. 17 and in $\mathbb{E}[F_T]$.

Additional parallel experiments may show consistent evidence of coupling; thus, we investigate the distribution of delay times $\rho(\Delta T)$ as $p$ is varied. Fig. 5 *D* shows $\rho(\Delta T)$ rescaled so that the largest value is set to unity for easier visualization. We see that for intermediate values of $10 \lesssim p \lesssim 13$ (unit codons/s, omitted henceforth), $\rho(\Delta T)$ can be bimodal. Fig. 5 *E* depicts a single peaked $\rho(\Delta T)$ when coupling is completely turned off by setting $k_a = 0, (E_a = -\infty)$. In this case, $\ell$ is irrelevant. Fig. 5 *F* shows the rescaled $\rho(\Delta T)$ in the presence of coupling ($E_a = 3$) for $\ell = 40$. Here, there are two regimes, $8 \lesssim p \approx 12$ and $18 \lesssim p \lesssim 24$, that exhibit bimodality. The delay-time density would be ideally measured via single-molecule or single-cell experiments combined with proper fluorescent imaging. However, in Appendix S7 we also consider how improved bulk LacZ completion assays can be used to estimate features of $\rho(\Delta T)$. We find that the distribution of ribosome completion times $T_{\rm rib}$ is always mono-modal and that the bimodality of $\Delta T$ is mainly the result of bimodality in $T_{\rm RNAP}$.

## Genome-wide variability of coupling

We have so far assumed all parameters are homogeneous along the transcript and time independent. However, a cell is able to dynamically regulate the transcription and translation of different genes by exploiting the transcript sequence or other factors that mediate the process. Such regulation can be effectively described within our model by varying its parameters in the appropriate way.

### *Regulation of RNAP pausing*

The RNAP pausing rate $k_-$ is one parameter that can be modulated by specific DNA sequences and other roadblocks along the gene (36,41–43). There is evidence that consensus pause sequences are enriched at the beginning of genes (44,45). In addition to leading ribosomes, a trailing RNAP can also push the leading RNAP out of a paused state by increasing $k_+$, much like ribosomes (6,36). Even if $k_+$ and $k_-$ are varied in our model, the overall predicted performance regimes of the system are still delineated by values of $p/\overline{q}$, and the effective transcription velocity can still be predicted by Eq. 17.

### *Effects of translation initiation rates*

Translation initiation is another process that can be altered by the cell through, e.g., initiation factors that modulate the initiation rate $\alpha$ (46). Genome-wide analysis reveals that translation initiation times in *E. coli* are highly variable, ranging from less than 1 s to more than 500 s (31,47).

As shown in Figs. S8 *A–C* of Appendix S8, varying the translation initiation rate $\alpha$ straightforwardly affects TTC. As indicated in (*A*), the peak in $\overline{V}_{\mathrm{RNAP}}$ at $\alpha \simeq 1/\mathrm{s}$ persists across different values of $p$. Slower translation initiation results in larger initial separations $n_0$, decreasing the overall fraction of protected times, as shown in (*B*) and (*C*). To mitigate large initial distances $n_0$ and lower likelihood coupling due to slow initiation, RNAP pausing occurs more often at the start of the gene to allow time for a slow-initiating ribosome to catch up. Thus, delayed ribosome initiation and early RNAP pausing are two "opposing" processes that can regulate coupling and efficiency, especially for short genes.

A simple analytic description of how the interplay between length $L$ and transcription initiation rate $\alpha$ affects our TTC metrics could not be found. However, large/small $\alpha$ generally leads to higher/lower $C$ and $\mathbb{E}[F_T]$ compared with those associated with the $L \to \infty$ approximations (Eqs. 15 and 16), as shown in Fig. S9 in Appendix S8. For sufficiently small $\alpha$, a rough estimate of the deviation from steady state is $p\overline{q}/[(p - \overline{q})\alpha L]$, the typical time needed for the ribosome to catch up to the RNAP divided by the time needed for the RNAP to finish the transcription.

### *Ribosome translocation rate profiles*

Although we have thus far assumed uniform ribosome translocation rates, it is known that codon bias and tRNA/amino acid availability can locally affect ribosome translocation (20,48). Snapshots of ribosome positions along transcripts have been inferred from ribosome profiling experiments. After imposing a stochastic exclusion model (49), Khanh and coworkers (50) reconstructed position-dependent ribosome translocation rates $p_m$. They found that hopping rates $p_m$ are larger near the 5′ end and decrease toward the 3′ end. Although they reconstructed the entire genome-wide $p_m$ profile, translocation rates are gene dependent, so we will propose and test simple profiles $p_m$.

To qualitatively match the inferred profile (50), we define profile 1 by increasing $p$ by 50% for the first 40 codons, and decreasing it by 50% for the second 40 codons. The rest of the transcript retains the constant baseline value of $p$. Profile 2 is similarly defined except that, instead of being the second group of 40 codons, the speed across the last 40 codons is decreased. We compared the performance of the three different profiles in Fig. S8 *D–F* as a function of the mean translation rate $\overline{p} \equiv L^{-1}\sum_{m=1}^{L} p_m$. We conclude that the differences in the effective velocities and protection fraction are subtle, suggesting that these performance statistics are relatively insensitive to different speed profiles.

## CONCLUSIONS

We have presented a detailed stochastic model of TTC. The continuous-time discrete-state model tracks the distance between the leading ribosome and the RNAP and assumes they sterically exclude each other along the nascent mRNA transcript. All current experimental understanding of interactions between RNAP and ribosome, including ribosome initiation, RNAP pausing, and direct ribosome-RNAP association, have also been incorporated. Our model exhibits a number of rich features that depend on the interplay of these intermediate mechanisms.

To quantitatively investigate the predictions of our model, we constructed three different metrics to quantify TTC, the delay-time probability distribution $\rho(\Delta T)$, the probability $C$ that the ribosome and the RNAP are in a bound state $(a = 1)$ at termination, and the fraction of time $F_T$ that the ribosome and the RNAP are proximal over the entire process. $F_T$ is a measure of protection against binding of termination proteins. These metrics were computed or simulated under different model parameters. Specifically, since a bound RNAP at distance $\ell$ from the trailing ribosome needs to first detach before $d = \ell$ can be increased, the $d \leq \ell$ states shown in Figs. 2 and S1 form an effective attractive well that tethers RNAP to ribosome. By allowing direct ribosome-RNAP binding, we find that this effective attraction zone can allow a slower ribosome to dynamically hold back bound RNAP, leading to decreased $\overline{V}_{\mathrm{RNAP}}$. Indirect coupling mediated by Nus proteins provides a longer interaction range, which may improve translation efficiency $\eta$ compared with direct coupling where $\ell \sim 4$ codons.

Qualitatively, our model predicts two different regimes of TTC that appear to be consistent with observations. One limit can arise when $E_a$ is large, resulting in close proximity and strong molecular coupling that may lead to slowdown of RNAP, while the other arises when $E_a$ is small leading to intermittent contacts and perhaps modest speed up of pausing RNAPs. Besides $E_a$, our model suggests that $\ell$, $\alpha$, and $p/\overline{q}$ also control which type of TTC arises. Across different genes, $E_a$ and $\ell$ are expected to be unchanged, but variations in $p/\overline{q}$ (and to some degree $\alpha$) can affect the balance between these qualitative models of TTC. Our analysis suggests that the unstalling enhancement $E_+$ is a key factor determining how TTC is manifested. For inefficient unstalling, increased coupling slows down the whole expressome, which might be disadvantageous under growth conditions. Gene-dependent kinetic parameters and signaling pathways involving ppGpp (12,22) and other factors can also be incorporated into our model to provide a more complete picture of how TTC influences cellular regulation.

Our model reveals that a bimodal time-delay distribution when $p \approx \overline{q}$ is a hallmark of molecular association. We provide a discussion of possible measurements of this distribution through traditional bulk assays in the supporting material. By quantitatively controlling ribosome speed $p$ and measuring the corresponding effective velocity measured in the LacZ-completion assay or other single-molecule assays. such as DNA curtains, important kinetic information associated with the delay-time density may be revealed by fitting our model to data.

Measurement of important parameters and indices, such as $E_+$ and $F_T$, could be obtained from quantitative analysis of previous experiments (2,22). Cryo-EM approaches used in (17) might also be used to obtain a genome-wide estimate of the coupling coefficient $C$. Finally, FRET experiments or super-resolution imaging may shed light on macromolecular-level ribosome and RNAP dynamics (51). Our model can guide how in vitro measurements can be designed and used to inform delay-time distributions $\rho(\Delta T)$, coupling coefficients $C$, protected-time fractions $F_T$, and efficiencies $\eta$.

Modeling of transcription and translation coupling may also inform the stochastic modeling of gene transcription dynamics. Simple kinetic models of transcription that incorporate the active and inactive states of the gene, the transcription initiation, elongation, pausing, premature termination, and the degradation of mRNA products have been developed to understand cell-to-cell variability of gene-specific mRNA levels (52–54). Such models could be merged with our modeling approach to accommodate TTC.

## SUPPORTING MATERIAL

Supporting material can be found online at https://doi.org/10.1016/j.bpj.2022.09.041.

## AUTHOR CONTRIBUTIONS

X.L. and T.C. devised and analyzed the model and wrote the paper. X.L. developed the computational algorithms and performed the numerical calculations and kinetic Monte Carlo simulations.

## ACKNOWLEDGMENTS

This work was supported by grants from the NIH through grant R01HL146552 and the NSF through grant DMS-1814364 (to T.C.).

## DECLARATION OF INTERESTS

The authors declare no competing interests.

## REFERENCES

1. Miller, O. L., B. A. Hamkalo, and C. A. Thomas. 1970. Visualization of bacterial genes in action. *Science.* 169:392–395.
2. Stevenson-Jones, F., J. Woodgate, …, N. Zenkin. 2020. Ribosome reactivates transcription by physically pushing RNA polymerase out of transcription arrest. *Proc. Natl. Acad. Sci. USA.* 117:8462–8467.
3. Sydow, J. F., and P. Cramer. 2009. RNA polymerase fidelity and transcriptional proofreading. *Curr. Opin. Struct. Biol.* 19:732–739, Catalysis and regulation/Proteins.
4. Knippa, K., and D. O. Peterson. 2013. Fidelity of RNA polymerase II transcription: role of Rbp9 in error detection and proofreading. *Biochemistry.* 52:7807–7817.
5. Sahoo, M., and S. Klumpp. 2013. Backtracking dynamics of RNA polymerase: pausing and error correction. *J. Phys. Condens. Matter.* 25:374104.
6. Zuo, X., and T. Chou. 2022. Density- and elongation speed-dependent error correction in RNA polymerization. *Phys. Biol.* 19:026001.
7. Chalissery, J., G. Muteeb, …, R. Sen. 2011. Interaction surface of the transcription terminator Rho required to form a complex with the C-terminal domain of the antiterminator NusG. *J. Mol. Biol.* 405:49–64.
8. Lawson, M. R., W. Ma, …, J. M. Berger. 2018. Mechanism for the regulated control of bacterial transcription termination by a universal adaptor protein. *Mol. Cell.* 71:911–922.e4.
9. Kohler, R., R. A. Mooney, …, P. Cramer. 2017. Architecture of a transcribing-translating expressome. *Science.* 356:194–197.
10. Ma, C., M. Mobli, …, P. J. Lewis. 2015. RNA polymerase-induced remodelling of NusA produces a pause enhancement complex. *Nucleic Acids Res.* 43:2829–2840.
11. Proshkin, S., A. R. Rahmouni, …, E. Nudler. 2010. Cooperation between translating ribosomes and RNA polymerase in transcription elongation. *Science.* 328:504–508.
12. Iyer, S., D. Le, B. R. Park, and M. Kim. 2018. Distinct mechanisms coordinate transcription and translation under carbon and nitrogen starvation in Escherichia coli. *Nat. Microbiol.* 3:741–748.
13. Vogel, U., and K. F. Jensen. 1994. The RNA chain elongation rate in Escherichia coli depends on the growth rate. *J. Bacteriol.* 176:2807–2813.
14. Fan, H., A. B. Conn, …, G. M. Blaha. 2017. Transcription–translation coupling: direct interactions of RNA polymerase with ribosomes and ribosomal subunits. *Nucleic Acids Res.* 45:11043–11055.
15. Mooney, R. A., S. E. Davis, …, R. Landick. 2009. Regulator trafficking on bacterial transcription units in vivo. *Mol. Cell.* 33:97–108.
16. Saxena, S., K. K. Myka, …, M. E. Gottesman. 2018. Escherichia coli transcription factor NusG binds to 70S ribosomes. *Mol. Microbiol.* 108:495–504.
17. O'Reilly, F. J., L. Xue, A. Graziadei, L. Sinn, S. Lenz, D. Tegunov, C. Blötz, N. Singh, W. J. H. Hagen, P. Cramer, J. Stülke, J. Mahamid, and

J. Rappsilber. 2020. In-cell architecture of an actively transcribing-translating expressome. *Science.* 369:554–557.

18. Webster, M. W., M. Takacs, …, A. Weixlbaumer. 2020. Structural basis of transcription-translation coupling and collision in bacteria. *Science.* 369:1355–1359.
19. Burmann, B. M., K. Schweimer, …, P. Rösch. 2010. A NusE:NusG complex links transcription and translation. *Science.* 328:501–504.
20. Chou, T., and G. Lakatos. 2004. Clustered bottlenecks in mRNA translation and protein synthesis. *Phys. Rev. Lett.* 93:198101.
21. Chen, M., and K. Fredrick. 2018. Measures of single- versus multiple-round translation argue against a mechanism to ensure coupling of transcription and translation. *Proc. Natl. Acad. Sci. USA.* 115:10774–10779.
22. Zhu, M., M. Mori, …, X. Dai. 2019. Disruption of transcription–translation coordination in Escherichia coli leads to premature transcriptional termination. *Nat. Microbiol.* 4:2347–2356.
23. Washburn, R. S., P. K. Zuber, …, J. Frank. 2020. Escherichia coli NusG links the lead ribosome with the transcription elongation complex. *iScience.* 23:101352.
24. Mäkelä, J., J. Lloyd-Price, …, A. S. Ribeiro. 2011. Stochastic sequence-level model of coupled transcription and translation in prokaryotes. *BMC Bioinf.* 12:121–213.
25. Johnson, G. E., J.-B. Lalanne, …, G.-W. Li. 2020. Functionally uncoupled transcription–translation in Bacillus subtilis. *Nature.* 585:124–128.
26. Li, R., Q. Zhang, …, H. Shi. 2016. Effects of cooperation between translating ribosome and RNA polymerase on termination efficiency of the Rho-independent terminator. *Nucleic Acids Res.* 44:2554–2563.
27. Chou, T. 2007. Peeling and sliding in nucleosome repositioning. *Phys. Rev. Lett.* 99:058105.
28. Teimouri, H., C. Spaulding, and A. B. Kolomeisky. 2022. Optimal pathways control fixation of multiple mutations during cancer initiation. *Biophys. J.* 121:3698–3705.
29. Wang, C., V. Molodtsov, …, R. H. Ebright. 2020. Structural basis of transcription-translation coupling. *Science.* 369:1359–1365.
30. Dai, X., M. Zhu, M. Warren, …, T. Hwa. 2016. Reduction of translating ribosomes enables Escherichia coli to maintain elongation rates during slow growth. *Nat. Microbiol.* 2:16231.
31. Shaham, G., and T. Tuller. 2018. Genome scale analysis of Escherichia coli with a comprehensive prokaryotic sequence-based biophysical model of translation initiation and elongation. *DNA Res.* 25:195–205.
32. Kennell, D., and H. Riezman. 1977. Transcription and translation initiation frequencies of the Escherichia coli lac operon. *J. Mol. Biol.* 114:1–21.
33. Xu, L., H. Chen, …, Z. W. Luo. 2006. Average gene length is highly conserved in prokaryotes and eukaryotes and diverges only between the two kingdoms. *Mol. Biol. Evol.* 23:1107–1108.
34. Young, R., and H. Bremer. 1976. Polypeptide-chain-elongation rate in Escherichia coli B/r as a function of growth rate. *Biochem. J.* 160:185–194.
35. Zhu, M., X. Dai, and Y.-P. Wang. 2016. Real time determination of bacterial in vivo ribosome translation elongation speed based on LacZα complementation system. *Nucleic Acids Res.* 44:e155.
36. Epshtein, V., and E. Nudler. 2003. Cooperation between RNA polymerase molecules in transcription elongation. *Science.* 300:801–805.
37. Neuman, K. C., E. A. Abbondanzieri, …, S. M. Block. 2003. Ubiquitous transcriptional pausing is independent of RNA polymerase backtracking. *Cell.* 115:437–447.
38. Bortz, A. B., M. H. Kalos, and J. L. Lebowitz. 1975. A new algorithm for Monte Carlo simulation of Ising spin systems. *J. Comput. Phys.* 17:10–18.
39. Gillespie, D. T. 1977. Exact stochastic simulation of coupled chemical reactions. *J. Phys. Chem. A.* 81:2340–2361.
40. Koslover, D. J., F. M. Fazal, …, S. M. Block. 2012. Binding and translocation of termination factor Rho studied at the single-molecule level. *J. Mol. Biol.* 423:664–676.
41. Komissarova, N., and M. Kashlev. 1997. RNA polymerase switches between inactivated and activated states by translocating back and forth along the DNA and the RNA. *J. Biol. Chem.* 272:15329–15338.
42. Nudler, E. 2009. RNA polymerase active center: the molecular engine of transcription. *Annu. Rev. Biochem.* 78:335–361.
43. Davenport, R. J., G. J. Wuite, …, C. Bustamante. 2000. Single-molecule study of transcriptional pausing and arrest by *E. coli* RNA polymerase. *Science.* 287:2497–2500.
44. Hatoum, A., and J. Roberts. 2008. Prevalence of RNA polymerase stalling at Escherichia coli promoters after open complex formation. *Mol. Microbiol.* 68:17–28.
45. Larson, M. H., R. A. Mooney, …, J. S. Weissman. 2014. A pause sequence enriched at translation start sites drives transcription dynamics in vivo. *Science.* 344:1042–1047.
46. Chou, T. 2003. Ribosome recycling, diffusion, and mRNA loop formation in translational regulation. *Biophys. J.* 85:755–773.
47. Siwiak, M., and P. Zielenkiewicz. 2013. Transimulation - protein biosynthesis web service. *PLoS One.* 8:e73943.
48. Klumpp, S., J. Dong, and T. Hwa. 2012. On ribosome load, codon bias and protein abundance. *PLoS One.* 7:e48542.
49. MacDonald, C. T., and J. H. Gibbs. 1969. Concerning the kinetics of polypeptide synthesis on polyribosomes. Biopolymers. *Biopolymers.* 7:707–725.
50. Dao Duc, K., and Y. S. Song. 2018. The impact of ribosomal interference, codon usage, and exit tunnel interactions on translation elongation rate variation. *PLoS Genet.* 14:e1007166.
51. Morisaki, T., K. Lyon, …, T. J. Stasevich. 2016. Real-time quantification of single RNA translation dynamics in living cells. *Science.* 352:1425–1429.
52. Choubey, S., J. Kondev, and A. Sanchez. 2015. Deciphering transcriptional dynamics in vivo by counting nascent RNA molecules. *PLoS Comput. Biol.* 11:e1004345.
53. Xu, H., S. O. Skinner, …, I. Golding. 2016. Stochastic kinetics of nascent RNA. *Phys. Rev. Lett.* 117:128101.
54. Filatova, T., N. Popovic, and R. Grima. 2020. Statistics of nascent and mature RNA fluctuations in a stochastic model of transcriptional initiation, elongation, pausing, and termination. *Bull. Math. Biol.* 83:3.

**Biophysical Journal, Volume *122***

## Supplemental information

# Stochastic dynamics and ribosome-RNAP interactions in transcription-translation coupling

**Xiangting Li and Tom Chou**

# SUPPLEMENTARY INFORMATION: MATHEMATICAL APPENDICES

## S1 Stochastic Simulations

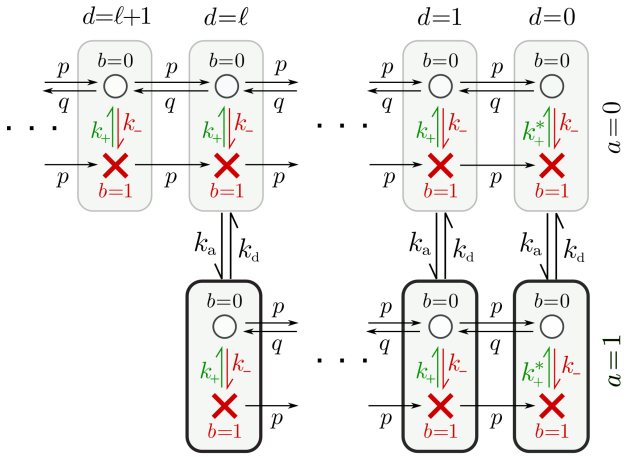


Figure S1: A more detailed schematic of the state space associated with different values of the ribosome-RNAP distance $d = n - m \lesssim \ell$. Open circles ($b = 0$) represent states with processing RNAP that allow $d$ to increase and decrease with rate $q$ and $p$, respectively. Processing states can transition with rate $k_-$ to states that contain a paused RNAP (red crosses, $b = 1$, $q = 0$). When $0 \le d \le \ell$, transitions between coupled and uncoupled states occur at rate $k_\mathrm{d}, k_\mathrm{a}$. When $d = \ell$ and $a = 1$, the coupled RNAP cannot proceed, even if it is processive, without first dissociating from the ribosome. Only after detachment ($a = 0$) can the separation exceed $\ell$, during which binding cannot occur and the ribosome and the RNAP process independently without the tethering constraint. Thus, bound states with $a = 1$ (and $0 \le d \le \ell$) describe a kinetic trap in which the ribosome and RNAP are tethered by the $\ell$-length mRNA and overall transcription can occur only through inchworming. Whether bound or unbound, when $d = 0$, the ribosome increases the RNAP unstalling rate from $k_+$ to $k_+^* = k_+ e^{E_+}$.

Although numerical and analytic evaluation of the master equation associated with our stochastic model is possible in some limits, certain quantities such as the fraction of protected time $F_T$ are most easily evaluated via Monte-Carlo simulation. Using the state space depicted in Figs. 2 and S1, and the rates defined in Eqs. 2–10, we implemented an event-based kinetic Monte Carlo algorithm to simulate trajectories of our full model. The Gillespie (39) or Bortz-Kalos-Lebowitz algorithm (38) first finds all the possible reactions and their rates. Then, one randomly chooses, with probability weighted by all the reaction rates, a reaction to fire. An independent random number is again drawn from the exponential distribution with rate equal to the total reaction rates. The relevant code is available at https://github.com/hsianktin/ttc.

## S2 Master equation

The probability of a state $\omega = (m, n, a, b) \in \Omega$ at time $t$ is defined by $\mathbb{P}_t(m, n, a, b) \equiv \mathbb{P}[\omega_t = (m, n, a, b)]$. Here, $\Omega$ is the sample space of all allowable $(m, n, a, b)$. Because the $(a, b) \in \{0, 1\}^2$ contains only four components, we can flatten the four-component probability $\mathbb{P}_t$ by introducing the $(m, n)$-dependent probability vectors $\mathbf{P}(m, n) = (P_0(m, n), P_1(m, n), P_2(m, n), P_3(m, n))^T$ in which the components describe the probabilities associated with the internal $(a, b)$ configurations when the ribosome and the RNAP are at positions $(m, n) \in \Omega_{mn}$:

- $P_0$: ribosome and RNAP are unassociated and both processing ($a = 0, b = 0$)
- $P_1$: processing ribosome, but paused, unassociated RNAP ($a = 0, b = 1$)
- $P_2$: associated ribosome/RNAP, both in processing states ($a = 1, b = 0$)
- $P_3$: associated ribosome/RNAP, paused RNAP ($a = 1, b = 1$)

The last two states can only arise when the ribosome and the RNAP are within the interaction range $d \equiv n - m \le \ell$.

The transition matrix describing transitions among elements of the $4 \times 1$ probability vector $\mathbf{P}$ are organized in terms of $4 \times 4$ matrices $\mathbf{p}_{m,n}$, $\mathbf{q}_{m,n}$, and $\mathbf{k}_{m,n}$

$$\mathbf{p}_{m,n} = \begin{pmatrix} p_m & 0 & 0 & 0 \\ 0 & p_m & 0 & 0 \\ 0 & 0 & p_m & 0 \\ 0 & 0 & 0 & p_m \end{pmatrix}, \quad \mathbf{q}_{m,n} = \begin{pmatrix} q_n & 0 & 0 & 0 \\ 0 & 0 & 0 & 0 \\ 0 & 0 & q_n \mathbb{1}_{d<\ell} & 0 \\ 0 & 0 & 0 & 0 \end{pmatrix}, \quad \mathbf{k}_{0,n} = \begin{pmatrix} -k_- & k_+ & 0 & 0 \\ k_- & -k_+ & 0 & 0 \\ 0 & 0 & 0 & 0 \\ 0 & 0 & 0 & 0 \end{pmatrix}$$

$$\mathbf{k}_{m\geq 1,n} = \begin{pmatrix} -k_- - k_\mathrm{a}(m,n) & k_+ & k_\mathrm{d} & 0 \\ k_- & -k_+ - k_\mathrm{a}(m,n) & 0 & k_\mathrm{d} \\ k_\mathrm{a}(m,n) & 0 & -k_- - k_\mathrm{d} & k_+ \\ 0 & k_\mathrm{a}(m,n) & k_- & -k_+ - k_\mathrm{d} \end{pmatrix}, \tag{S1}$$

$$\mathbf{k}_{n,n} = \begin{pmatrix} -k_- - k_\mathrm{a} & k_+^* & k_\mathrm{d} & 0 \\ k_- & -k_+^* - k_\mathrm{a} & 0 & k_\mathrm{d} \\ k_\mathrm{a} & 0 & -k_- - k_\mathrm{d} & k_+^* \\ 0 & k_\mathrm{a} & k_- & -k_+^* - k_\mathrm{d} \end{pmatrix},$$

where $\mathbf{p}_{m,n}$ and $\mathbf{q}_{m,n}$ contain processive ribosome and processive RNAP hopping rates and $\mathbf{k}_{m,n}$ is the transition rate matrix connecting the internal ribosome/RNAP states. Here, $\mathbb{1}_z = 1$ if and only if condition $z$ is satisfied, $\mathbb{1}_z = 0$ otherwise. Ribosome-RNAP exclusion is imposed via $\mathbf{p}_{n,n} = 0$ and ribosome initiation is defined by $p_{m=0} \equiv \alpha$. The internal-state conversion rate matrix depends on $(m,n)$ via $k_\mathrm{a}(m,n) = k_\mathrm{a}\mathbb{1}_{d\leq\ell}$. For simplicity, we assume the values of the intrinsic kinetic rates $k_\pm$, $k_\mathrm{a,d}$ to be otherwise $(m,n)$-independent (although $p_m$ and $q_n$ can still depend on position). The master equation is then given by

$$\frac{\partial \mathbf{P}(m,n)}{\partial t} = \mathbf{p}_{m-1,n}\mathbf{P}(m-1,n) + \mathbf{q}_{m,n-1}\mathbf{P}(m,n-1) - (\mathbf{p}_{m,n} + \mathbf{q}_{m,n})\mathbf{P}(m,n) + \mathbf{k}_{m,n}\mathbf{P}(m,n), \quad 0 \leq m \leq n, \tag{S2}$$

with boundary conditions $\mathbf{P}(-1,n) = \mathbf{P}(m,-1) = \mathbf{P}(m,n)|_{m>n} = 0$. For time-homogeneous problems, we define the time Laplace-transformed probability vector $\mathcal{L}\{P(m,n,t)\} \equiv \tilde{\mathbf{P}}_{m,n}(s)$, which satisfies

$$s\tilde{\mathbf{P}}_{m,n} - \mathbf{P}(m,n,t=0) = \mathbf{p}_{m-1,n}\tilde{\mathbf{P}}_{m-1,n} + \mathbf{q}_{m,n}\tilde{\mathbf{P}}_{m,n-1} - (\mathbf{p}_{m,n} + \mathbf{q}_{m,n})\tilde{\mathbf{P}}_{m,n} + \mathbf{k}_{m,n}\tilde{\mathbf{P}}_{m,n}. \tag{S3}$$

We set the initial condition $P_i(m,n,t=0) = \delta_{m,0}\delta_{n,1}\delta_{i,1}$ ($\delta_{ij}$ is the Kronecker $\delta$-function) to describe a ribosome-free system immediately after a processing RNAP has started transcription. The probability of this state is then self determined by $\tilde{\mathbf{P}}_{0,1}(s) = \boldsymbol{\gamma}_{0,1}^{-1}(s)\mathbf{e}_1$ where $\mathbf{e}_1 = (1,0,0,0)^T$ and $\boldsymbol{\gamma}_{0,1}(s) = (s\mathbf{I} + \mathbf{p}_0 + \mathbf{q}_{0,1} - \mathbf{k}_{0,1})$, where $\mathbf{I}$ is the identity matrix. Starting from this value, we can evaluate the vector recursion relation in Eq. S3. Be defining $\boldsymbol{\gamma}_{m,n} \equiv (s\mathbf{I} + \mathbf{p}_{m,n} + \mathbf{q}_{m,n} - \mathbf{k}_{m,n})$, the recursion relation is simplified to

$$\tilde{\mathbf{P}}_{m,n} = \boldsymbol{\gamma}_{m,n}^{-1}\left[\mathbf{p}_{m-1,n}\tilde{\mathbf{P}}_{m-1,n} + \mathbf{q}_{m,n-1}\tilde{\mathbf{P}}_{m,n-1}\right]. \tag{S4}$$

$\tilde{\mathbf{P}}_{m,n}$ is explicitly solved by

$$\tilde{\mathbf{P}}_{m,n} = \sum_{\theta\in\Theta} \mathbf{p}^m \mathbf{q}^{n-1} \prod_{i=2}^{m+n-1} \boldsymbol{\gamma}_{\theta_i}^{-1}\tilde{\mathbf{P}}_{0,1}, \tag{S5}$$

where $\Theta$ is the set of all possible paths $\theta = (\theta_1, \ldots, \theta_{m+n-1})$ connecting $(0,1)$ to $(m,n)$.

The recursion relation Eq. S4 can be evaluated numerically to find $\tilde{\mathbf{P}}_{m,n}$, while the path integral Eq. S5 can be used to approximate analytic solutions in specific limits. For example, if there is no ribosome-RNAP binding, and all other parameters are homogeneous, $\tilde{P}_3 = \tilde{P}_4 = 0$. We can project all parameters and variables into a two-dimensional subspace supported by $\left\{\tilde{P}_0, \tilde{P}_1\right\}$. The only interactions considered are the volume exclusion effects. In this case, $\boldsymbol{\gamma}$ assumes two possible values. In the interior $(m < n)$, $\boldsymbol{\gamma}_\mathrm{in} = (s\mathbf{I} + \mathbf{p} + \mathbf{q} - \mathbf{k})$ while on the boundary $\partial\Omega_{mn} \equiv \{(m,n) \in \Omega_{mn} : m = n\}$, $\boldsymbol{\gamma}_\mathrm{ex} = (s\mathbf{I} + \mathbf{q} - \mathbf{k})$. We can classify different paths $\theta$ by the number of visits $w$ to the boundary before reaching $(m,n)$: $\Theta_w \equiv \{\|\{\theta_i\}_{i=1}^{\|\theta\|-1} \cap \partial\Omega\| = w\}$. Eq. S5 can then be rearranged to

$$\tilde{\mathbf{P}}_{m,n} = \sum_{w=0}^{\infty} \sum_{\theta\in\Theta_w} \mathbf{p}^m \mathbf{q}^{n-1} \boldsymbol{\gamma}_\mathrm{ex}^{-w} \boldsymbol{\gamma}_\mathrm{in}^{-(m+n-1-w)} \tilde{\mathbf{P}}_{0,1} \tag{S6}$$

**Analytic solution for the first passage problem.** A simpler closed-form analytic solution can be obtained when considering a first passage problem to the boundary $\partial\Omega_{mn}$. If $\omega_t$ denotes the stochastic process of the TTC problem, we wish to find the probability that the position $\omega_t$ at time $t$ is $(m,n)$ and that at $T_\mathrm{b} \geq t$: $\mathbb{P}(\omega_t = (m,n), T_\mathrm{b} \geq t)$. To solve this problem, we use the method of coupling. Consider a second, absorbing process $\omega'_t$ which is coincidental with $\omega_t$ up until $T_\mathrm{b}$, upon which it ceases to evolve. In other words, $\omega'_t = \omega_{\min\{t,T_\mathrm{b}\}}$. For the $\omega'_t$ process, the Laplace-transformed probability satisfies

$$\tilde{\mathbf{P}}_{m,n} = \sum_{\theta\in\Theta_0} \mathbf{p}^m \mathbf{q}^{n-1} \gamma_\mathrm{in}^{-(m+n-1)} \tilde{\mathbf{P}}_{0,1}. \tag{S7}$$

Note that each term in the summation does not depend on the actual path $\theta \in \Theta_0$. Therefore, we just need to calculate the size of $\Theta_0$, which is a generalized problem of finding Catalan numbers. Obviously, when $m < n-1$, the size is simply the binomial coefficient $\binom{m+n-1}{m}$.

To proceed further, we need to further assume $\ell = 1$ before calculating powers of the truncated $2\times 2$ matrices $\boldsymbol{\gamma}_\mathrm{in}$ by first diagonalizing

$$\boldsymbol{\gamma}_\mathrm{in} = \begin{pmatrix} s+p+q+k_- & -k_+ \\ -k_- & s+p+k_+ \end{pmatrix} = \mathbf{V}^{-1}\mathbf{D}\mathbf{V}, \tag{S8}$$

where

$$\begin{aligned} \mathbf{V} &= \begin{bmatrix} \dfrac{-k_- + k_+ - q + \delta}{2k_-} & \dfrac{-k_- + k_+ - q - \delta}{2k_-} \\ 1 & 1 \end{bmatrix}, \\ \mathbf{D} &= \mathrm{diag}\left[ s + \frac{k_-}{2} + \frac{k_+}{2} + p + \frac{q}{2} - \frac{\delta}{2},\ s + \frac{k_-}{2} + \frac{k_+}{2} + p + \frac{q}{2} + \frac{\delta}{2} \right], \\ \delta &\equiv \sqrt{k_-^2 + 2k_-k_+ + 2k_-q + k_+^2 - 2k_+q + q^2}. \end{aligned} \tag{S9}$$

Then, $\boldsymbol{\gamma}_\mathrm{in}^n = \mathbf{V}^{-1}\mathbf{D}^n\mathbf{V}$ for all $n \in \mathbb{N}$. The $\mathbf{p}$ and $\mathbf{q}$ matrices are both diagonal, and their powers are straightforward to calculate. Thus, as long as the combinatoric factors can be calculated, Eq. S6 and S7 can be expressed in analytic forms.

## S3 Numerical procedure for conditional distributions

We also developed an iterative numerical algorithm for numerically approximating the probability distribution of the ribosome location $m$, the RNAP position, the RNAP state $b$, and the ribosome-RNAP association state $a$. The algorithm is detailed below. Again, use $\omega_t$ to denote the full state $(m_t, n_t, a_t, b_t)$ of the system at time $t$. Let $\tau_0 = 0$, and recursively define $\tau_n$ as

$$\tau_n = \inf\left\{ t > \tau_{n-1} : \omega_t \neq \omega_{\tau_{n-1}} \right\}. \tag{S10}$$

$\tau_n$ is the moment when the system leaves the current state $\omega_{\tau_{n-1}}$. When $\tau_{n-1} \leq t < \tau_n$, the system has yet to leave the state $\omega_{\tau_{n-1}}$. Therefore, $\omega_t = \omega_{\tau_{n-1}}$. Let $\mathbf{w}_n = \omega_{\tau_n}$. Then, the stopped process $\{\mathbf{w}_n\}_{n=0}^\infty$ is a discrete Markov chain on the same state space $\Omega$ as $\omega_t$ and its transition probabilities are given by

$$\mathbb{P}(\mathbf{w}_n | \mathbf{w}_{n-1}) = \frac{r(\mathbf{w}_n|\mathbf{w}_{n-1})}{\sum_{\omega\in\Omega} r(\omega|\mathbf{w}_{n-1})}, \quad \forall\, n \geq 1 \tag{S11}$$

where $r(\omega|\mathbf{w}_{n-1})$ is defined in Eqs. 2–10. This discrete Markov chain $\{\mathbf{w}_n\}$ precisely captures each jump between different states in the original process $\{\omega_t\}$. And it allows us to derive the probability distribution of $\mathbf{w}_{n+1}$ from that of $\mathbf{w}_n$ by a simple matrix multiplication.

In order to find the distribution of ribosome positions $m$ upon completion of transcription at time $T_\mathrm{RNAP}$, we first define the stopping times $t_k$ as the discrete-time analog of $T_k$ such that $\mathbf{w}_{t_k} = \omega_{T_k}$, where $T_k$ refers to the first time the RNAP reaches position $k$ as defined in the main text. The equality $\mathbf{w}_{t_k} = \omega_{T_k}$ implies that in order to characterize the distribution $\mathbb{P}(m,a,b \mid t = T_n)$ of $\omega_{T_n}$, we can characterize the distribution of $w_{t_n}$ instead:

$$\mathbb{P}(m,a,b \mid t = T_n) \equiv \mathbb{P}(\omega_{T_n} = (m,n,a,b)) = \mathbb{P}(\mathbf{w}_{t_n} = (m,n,a,b)). \tag{S12}$$

The sequence of stopping times $\{t_k\}_{k=1}^L$ admits the following properties: (a) for all $k \geq 1$, the stopping time $t_k$ is almost surely finite. (b) the sequence is monotonically increasing: $t_1 < t_2 < \cdots < t_L$. These two properties reveal that for all $k \geq 1$, $\lim_{j\to\infty} t_k + j > t_{k+1}$.

Consequently, if we define $t_k^{(j)} := \min\{t_k + j, t_{k+1}\}$, then for fixed $k$, $t_k^{(j)}$ converges pointwise to $t_{k+1}$ as $j \to \infty$. This convergence relation in turn guarantees

$$\lim_{j\to\infty} \mathbb{P}(\mathbf{w}_{t_k^{(j)}} = (m, k+1, a, b)) = \mathbb{P}(\mathbf{w}_{t_{k+1}} = (m, k+1, a, b)) \tag{S13}$$

since $\mathbb{P}(\mathbf{w}_{t_k^{(j)}} \neq \mathbf{w}_{t_{k+1}}) \leq \mathbb{P}(t_k^{(j)} \neq t_{k+1}) \to 0$, as $j \to \infty$. Inserting Eq. S12 into Eq. S13, we have

$$\lim_{j\to\infty} \mathbb{P}(\mathbf{w}_{t_k^{(j)}} = (m, k+1, a, b)) = \mathbb{P}(m, a, b \,|\, t = T_{k+1}), \tag{S14}$$

which allows us to approximate the distribution of $\mathbf{w}_{t_{k+1}}$ by the distribution of $\mathbf{w}_{t_k^{(j)}}$ when $j$ is large enough. The distribution of $\mathbf{w}_{t_k^{(j)}}$ is easy to calculate. Note that $\mathbf{w}_{t_k^0} = \mathbf{w}_{t_k}$, whose distribution is assumed to be known from iteration.

By the definition of the stopping time $t_k^{(j)}$, we observe that

$$\mathbf{w}_{t_k^{(j+1)}} = \begin{cases} \mathbf{w}_{t_k^{(j)}+1} & \text{if } t_k^{(j)} \neq t_{k+1}, \\ \mathbf{w}_{t_k^{(j)}} & \text{otherwise.} \end{cases} \tag{S15}$$

Therefore, the conditional probability that a sample path at time $t_k^{(j+1)}$ is in the state $\mathbf{w}_{t_k^{(j+1)}}$ provided that the sample path at time $t_k$ is in the state $\mathbf{w}_{t_k^{(j)}}$ is given by

$$\mathbb{P}(\mathbf{w}_{t_k^{(j+1)}} \mid \mathbf{w}_{t_k^{(j)}}) = \begin{cases} \mathbb{P}(\mathbf{w}_{t_k^{(j)}+1} \mid \mathbf{w}_{t_k^{(j)}}) & \text{if } t_k^{(j)} \neq t_{k+1}, \\ 1 & \text{if } t_k^{(j)} = t_{k+1} \text{ and } \mathbf{w}_{t_k^{(j)}} = \mathbf{w}_{t_k^{(j+1)}}, \\ 0 & \text{if } t_k^{(j)} = t_{k+1} \text{ and } \mathbf{w}_{t_k^{(j)}} \neq \mathbf{w}_{t_k^{(j+1)}}, \end{cases} \tag{S16}$$

where $\mathbb{P}(\mathbf{w}_{t_k^{(j)}+1} \mid \mathbf{w}_{t_k^{(j)}})$ is already given by Eq. S11. Finally, upon inserting Eq. S16 into

$$\mathbb{P}\left(\mathbf{w}_{t_n^{(k+1)}}\right) = \sum_{\mathbf{w}_{t_k^{(j)}}} \mathbb{P}(\mathbf{w}_{t_k^{(j+1)}} \mid \mathbf{w}_{t_k^{(j)}}) \mathbb{P}(\mathbf{w}_{t_k^{(j)}}), \tag{S17}$$

we obtain an iterative update law for the probability distribution of $\mathbf{w}_{t_k}^{(j)}$ in $j \geq 0$.

We approximate $\mathbb{P}(m, a, b \,|\, t = T_{n+1})$ by the distribution of $\mathbf{w}_{t_n^{(k)}}$ for sufficiently large $k$ and thus reconstruct $\mathbb{P}(m, a, b, | \, t = T_{n+1})$ from $\mathbb{P}(m, a, b, | \, t = T_n)$. We iterate this procedure until $\mathbb{P}(m, a, b, | \, t = T_L)$ is found. The distribution $\rho(\Delta T)$ is then found by multiple convolutions of the exponential distributions with rates $p_m, \ldots, p_L$, weighted by the probabilities $\mathbb{P}(m, a, b \,|\, t = T_L)$ over each $m, a, b$:

$$\rho(\Delta T) = \sum_m \mathbb{P}(m(T_{\text{RNAP}})) \left[ \circledast_{j=m}^{L} e^{-p_j t} \right] (\Delta T) \tag{S18}$$

where $\circledast_{j=m}^{L} f_j$ represents sequential convolutions of functions $\{f_j\}_{j=m}^{L}$; here, $f_j(t) = e^{-p_j t}$. An implementation of the above algorithm in Julia is available at https://github.com/hsianktin/ttc.

## S4 Steady-state approximation in the large system size limit

In the limit $L \to \infty$, we can analyze the system in a steady-state limit to find a number of useful analytic results. If we use the "center-of-mass" reference frame, we characterize the system by the distance $d = n - m$ between the leading ribosome and RNAP. The dynamics are described by a Markov process on the state space $(d, a, b)$ described in Fig. S1. In these variables, the continuous-time Markov chain admits an equilibrium distribution $\pi$ and is assumed to be ergodic in the sense that the fraction of time the system spends at a certain state $A$ is asymptotically equal to $\pi(A)$. This ergodicity allows us to find the effective velocity $\overline{V}$ and the fraction of protected time $F_T$.

With each state $(d, a, b)$ we can associate instantaneous ribosome and RNAP speeds $V_{\text{rib}}$ and $V_{\text{RNAP}}$ by the rates of decreasing and increasing $d$ by one codon, respectively. For example, $V_{\text{RNAP}}(d = \ell, 1, 0) = V_{\text{RNAP}}(d, a, 1) = 0$. Since ergodicity allows us to find the fraction of time the system is in state $A$ by its equilibrium probability $\pi(A)$, the effective velocity can be found by weighting $V_i(A), i \in \{\text{RNAP}, \text{rib}\}$ weighted by $\pi(A)$. Therefore, at equilibrium, the effective velocity coincides with the corresponding expected velocity.

A sample trajectory of $d$ as a function of time is shown in Fig S2A and B. When the ribosome and RNAP are close ($d \leq \ell$), they can transiently bind and unbind, with dwell times in each state controlled by $k_{\mathrm{a,d}}$. When the RNAP is processive, the ribosome lags behind. If the RNAP pauses for a sufficient time, the ribosome catches up and $d \simeq 0$. Under our specific set of parameters (large $E_{\mathrm{a}}$ and $\bar{q} < p < q$), $d = \ell$ over most of the trajectory. Recall that the coupling constraint prevents the distance to be larger than $\ell$ when ribosome is bound to RNAP. If $d > \ell$, ribosome and RNAP proceed independently. Fig. S2A-B

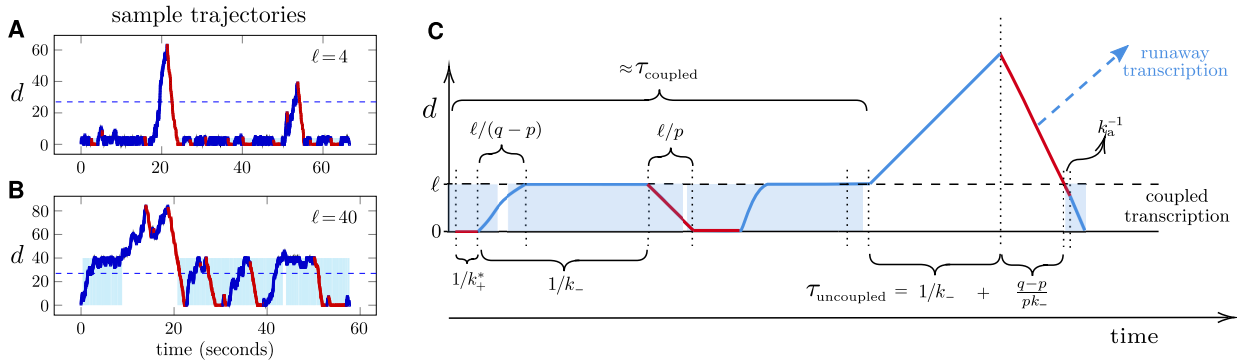


Figure S2: (A) A sample trajectory of distance $d$ between ribosome and RNAP as a function of time $t$, with $\ell = 4$, $L = 1000$, and all other parameters equivalent to those used in to generate Fig. 3. (B) A sample trajectory when the interaction distance is increased to $\ell = 40$, relevant for example, if an intermediate protein such as NusG is involved in forming the ribosome-RNAP expressome complex. In (A) and (B), blue(red) segments indicate processing(stalled) RNAP. The light-blue shaded regions indicate bound ribosome-RNAP complexes. (C) Schematic description of distances and estimates of transition rates. These estimates assume that microstates within a macrostate has reached steady state in $(d, a, b)$-space and will aid in deriving our analytic approximations.

motivates us to lump all the different states of the system into four representative groups of microstates:

- The paused, separated state ($d > \ell, b = 1$).
- The processive, separated state ($d > \ell, b = 0$).
- The paused, proximal state, ($d \leq \ell, b = 1$ and $a = 1$ most of the time).
- The processive, proximal state, ($d \leq \ell, b = 0$ and $a = 1$ most of the time).

In the following, we call these four lumped states as "macrostates," and the states within each macrostate as "microstates." Figure S2C provides the scaling of some quantities as the system explores these macrostates. Eventually, we will further simplify our approximations by lumping some macrostates into "metastates" as outlined in Fig. S3.

**Traffic jam in associated, processive states.** As an example of a calculation of transition rates and velocities, consider the details of the expected velocity of a coupled, processive expressome. In this particular case, the ribosome and RNAP intermittently touch ($d = 0$) each other. Therefore, they should have the same effective velocity $\overline{V}$. Suppose that the bound ribosome is slower than the processing RNAP, $p < q$. The average speed of the bound RNAP is thus limited by the speed of ribosome. However, the ribosome translocates at speed less than $p$ since it is occasionally blocked by the RNAP. The equilibrium probability that RNAP and ribosome are in contact ($d = 0$) is given by

$$\pi(d = 0 \,|\, a = 1, b = 0) = \frac{1}{\sum_{k=0}^{\ell} (q/p)^k}. \tag{S19}$$

By finding the complementary probability that $0 < d \leq \ell$, for which the ribosome can move forward with rate $p$, we find the expected expressome velocity

$$\mathbb{E}\left[V \,|\, a = 1, b = 0\right] = q \left[\frac{(q/p)^{\ell} - 1}{(q/p)^{\ell+1} - 1}\right]. \tag{S20}$$

Since $q \sim 30$ codons/s and $p \leq 15$ codons/s, $q/p \sim 2$ and the relative slowdown is sensitive to $\ell$ with small $\ell$ resulting in a significant slowdown of the expressome.

**Classification of different scenarios.** At equilibrium, if the average independent RNAP velocity $\bar{q}$ is smaller than $p$, the two machines will maintain a significant probability of proximity and coupling. However, if $p < \bar{q}$, the equilibrium ribosome-RNAP distance $d \to \infty$ and any interaction will vanish. Thus, we need only consider $p > \bar{q}$ and discuss the following scenarios:

1. The instantaneous speeds satisfy $p \geq q$. Then, the ribosome is always within close range of the RNAP and the system freely cycles among the four internal macrostates. We may assume that the binding and unbinding rates $k_a$ and $k_d$ are much larger than the pausing and unstalling rates $k_-$ and $k_+$.

2. The instantaneous speeds satisfy $p < q$ and the rate of uncoupling $k_d$ is slower than the rate of coupling $k_a$. This system maintains an appreciable probability of being coupled. When the RNAP is bound and processive, the distance quickly increases until $d \approx \ell$. Because $k_a > k_d$, the ribosome remains bound and maintains the distance $d \approx \ell$. During this period, the RNAP may pause and unpause a number of times before the ribosome unbinds. When the $d \leq \ell$ states are unbound, the ribosome can fall out of the interaction range $\ell$ and not able to immediately rebind. This gives rise to an effectively irreversible transition from a bound, processive state to an unbound, processive state. Rebinding can occur only after the RNAP again pauses, allowing the ribosome to catch up. Once this happens, the ribosome and RNAP will remain bound for a long time (since $E_a$ is large). It is also possible that before rebinding, the RNAP becomes processive again.

3. The instantaneous speeds satisfy $p < q$, but the dissociation rate $k_d$ is larger than the pausing rate $k_-$. This scenario is essentially the same as the previous one, with the only difference that the transition from the bound, processive state to an unbound processive state is fast and effectively irreversible.

These scenarios shown in Figs. S3A-C can be coarse-grained into common cyclic structures by grouping states by the underlying distance $d$ between RNAP and ribosome, as shown in Figs. S3D-F.

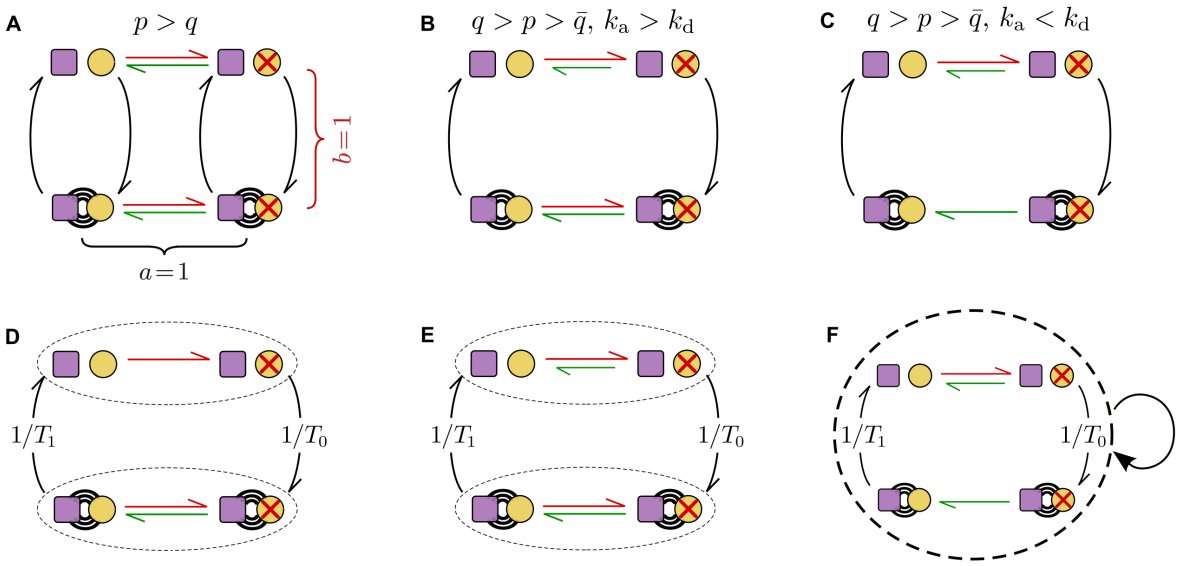


Figure S3: Coarse-grained states of the expressome. (A) A scenario in which binding and unbinding are relatively fast and that $p > q$ so that the ribosome is fast enough to fully allow binding. This case is rarely realized. (B) The limit in which binding is fast, but $\bar{q} < p < q$. In this case, when the two machines are close, they effectively remain bound. When the ribosome and RNAP are processive ($b = 1$), the ribosome is slower and held at a distance of $d \approx \ell$. If dissociation occurs, the ribosome lags behind out of the interaction range $\ell$ and cannot immediately rebind. The distance between the ribosome and the RNAP remains larger than $\ell$ until the RNAP pauses again and ribosome catches up. (C) Slow binding, fast unbinding regime that leads to only transient coupling. The slowdown of transcription is limited in this case. (D) The coarse-grained cyclic structure corresponding to the limit depicted in (A). (E) represents the coarse-grained cyclic structure corresponding to the limit shown in (B). (F) Coarse-grained cyclic structure associated with the limit in (C). In all scenarios, when the $d \leq \ell, a \approx 1$ states and the $d > \ell, a = 0$ states are respectively lumped together, common features arise in the transitions between the metastates. The system leaves the $d \leq \ell$ state always when the RNAP is processive and reenters this state always when the RNAP is stalled. By estimating the dwell times in each of these lumped metastates, $T_1$ and $T_0$ respectively, we can capture the most likely trajectories of the stochastic process.

For the different scenarios depicted in Fig. S3, the general approach is to estimate the transition rates between the $d > \ell$ metastate and the $d \leq \ell$ metastate under the assumption that $q > p > \bar{q}$. While there are experimental estimates of $E_a$ under certain circumstances, the absolute magnitude of $k_a$ is unknown. For the sake of simplicity, we assume a fast coupling and uncoupling regime where $k_a = 100/s \gg k_\pm$ Fortunately, upon using realistic parameter values, our metrics are rather insensitive to $k_a$ (and also $k_d$), as shown in Fig. S4 in which $E_a = 3$ was fixed. Since the $k_\pm \lesssim 1/s$, and $p, q \gtrsim 10$ codons/s, we also assume that $p, q \gg k_\pm$ in the following derivation.

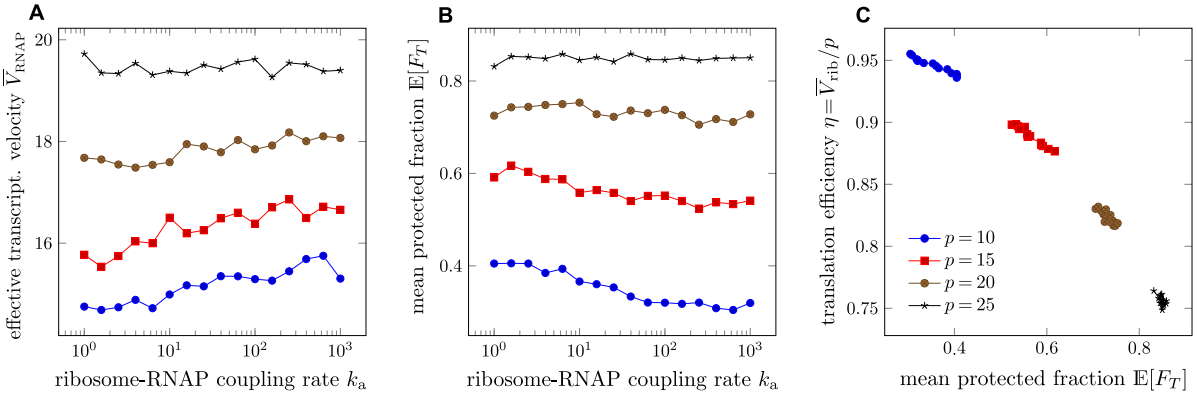


Figure S4: Effects of coupling rates $k_a$ while keeping $E_a = 3$, under varying values of $p$. Other unspecified parameters are set to those used in Fig. 3. (A) $\overline{V}_{\mathrm{RNAP}}$ as a function of $k_a$. (B) $\mathbb{E}[F_T]$ as a function of $k_a$. (C) Trade-off relation when $p$ and $k_a$ vary. The effects of $k_a$ are insignificant. All results are fairly insensitive to $k_a$ across multiple reasonable values of $p$.

Now, consider the metastate $d > \ell$. The system always enters this metastate first through $d = \ell + 1$ from a processive $d = \ell$ state. Starting from $d = \ell + 1$, it first monotonically increases linearly with rate $(q - p)$ for a time $1/k_-$. Then, after RNAP stalling, $d$ decreases linearly with rate $p$ for a time $1/k_+$. If $p/k_+ > (q - p)/k_-$, *i.e.*, $p > \bar{q}$, the system dwells in the $d > \ell$ metastate for a typical time $q/(pk_-)$ before exiting it.

However, since the transition between the paused and processive states of RNAP is stochastic, it is possible that the system does not enter $d \leq \ell$ state at the end of the first period of a paused RNAP. In order to account for this stochasticity, we first note that the main source of uncertainty is the exponentially distributed waiting time of state transitions of the RNAP, rather than the random forward hopping of the RNAP or ribosome. If $v$ is the instantaneous speed and $t$ is the total time passed, the standard deviation of the distance travelled by the random walk is $1/\sqrt{vt}$. In our model, $t \sim 1/k_\pm$ and $v \sim p, q$ satisfies $vt \gg 1$. Thus, the variability in the distance travelled by processive, unimpeded motors is negligible.

We decompose the dwell time into two components. The first component is the process of independent and identically distributed trials to enter $d \leq \ell$ within the first paused period of RNAP. These trials always start at $d = \ell + 1$. The number of trials in this case follows a geometric distribution, and the total time spent before entering the $d \leq \ell$ state is then $\frac{q}{pk_-} + (1/k_- + 1/k_+)\frac{(q-p)k_+}{pk_-}$. On the other hand, if a trial fails, with probability $1 - P_0 = 1 - [\frac{q}{pk_-} + (1/k_- + 1/k_+)\frac{(q-p)k_+}{pk_-}]$, the system enters another trial at the starting point $d > \ell + 1$. For a faraway starting point, we need additional cycles of pausing and unpausing to compensate for the drift. Conditioned on failure, the mean drift is still $(q - p)/k_-$ thanks to the memoryless property of exponential distribution. Each cycle on average reduces the drift by $p/k_+ - (q - p)/k_-$. We need then $\frac{(q-p)/k_-}{p/k_+-(q-p)/k_-}$ additional cycles with probability $(1-P_0)$. Each pausing-unpausing cycle takes an average of time $(1/k_-+1/k_+)$. After the extra cycles are consumed, the case falls back to the first component with the same total estimated time $\frac{q}{pk_-} + (1/k_- + 1/k_+)\frac{(q-p)k_+}{pk_-}$. In summary, with probability 1, there is a baseline dwell time $\frac{q}{pk_-} + (1/k_- + 1/k_+)\frac{(q-p)k_+}{pk_-}$ and with probability $(1 - P_0)$, there is an extra dwell time $(1/k_- + 1/k_+)\left[\frac{(q-p)/k_-}{p/k_+-(q-p)/k_-}\right]$. Consequently, the total time spent in the metastate $d > \ell$ is given by Eq. 11:

$$T_0 \approx \frac{q}{pk_-} + \left(\frac{1}{k_-} + \frac{1}{k_+}\right)\left[\frac{(q-p)k_+}{pk_-} + (1 - P_0)\frac{(q-p)/k_-}{p/k_+ - (q-p)/k_-}\right]$$

It is possible, when $p \lesssim q$, that $d \leq \ell$ even before the RNAP stalls. However, this scenario is unstable because the RNAP is still faster than the ribosome. The system will stay in the state for a small period of time and with a large probability it reenters the metastate $d > \ell$. We keep the limit $T_0 = 1/k_-$ when $p > q$. In the limit $p < \bar{q}$, since $p/k_+ < (q - p)/k_-$, the drift cannot be compensated by the cycles of pausing and unpausing, therefore we take $T_0 = +\infty$.

Next, we discuss the dwell time $T_1$ in the $d \le \ell$ metastate. $T_1$ can be similarly described in the form of an iid trial process. When $d \le \ell$, under the fast coupling assumption $k_a \gg k_\pm$, the system spends a fraction $k_a/(k_a + k_d)$ of time in the coupled state while the remaining time is spent in the uncoupled state. Simultaneously, the RNAP is processive for time $\sim 1/k_-$ and pauses for a duration $1/k_+^* + \ell/p$. The entry into $d \le \ell$ states occurs from $d = \ell$ when the RNAP is paused. Immediately after entry, $d$ will decrease to 0 as only the ribosome is processive. Once the RNAP becomes processive again $d$ must reach $\ell$ before dissociation. Using standard methods for a simple processive random walk, the time for $d = 0 \to d = \ell$ is given by $t_\ell = (1/p)(p/q)^\ell \sum_{j=1}^{\ell} j\,(q/p)^j$. The probability of leaving $d \le \ell$ from $d = \ell$ is roughly $q/(q+p)$. So, we need roughly $(q+p)/q$ trials and the system spends $\sim (q+p)t_\ell/q$ amount of time in the uncoupled, processive $(a, b) = (0, 0)$ state. Thus, probabilities in the $d \le \ell$ metastate can be decomposed into $\mathbb{P}(a = 0 \,|\, d \le \ell) \approx k_d/(k_a + k_d)$ and $\mathbb{P}(b = 0 \,|\, d \le \ell) \approx 1/(1 + k_-/k_+^* + k_-\ell/p)$. Under the assumption that $k_a$ is large, we can approximate $\mathbb{P}(a = 0, b = 0 \,|\, d \le \ell) \approx \mathbb{P}(a = 0 \,|\, d \le \ell)\mathbb{P}(b = 0 \,|\, d \le \ell)$ so that the total time spent in the metastate $d \le \ell$ is given by

$$T_1 \approx \mathbb{P}(a = 0, b = 0 \,|\, d \le \ell)^{-1} \frac{q+p}{q} t_\ell \approx \frac{k_a + k_d}{k_d} \left(1 + \frac{k_-}{k_+^*} + \frac{k_-\ell}{p}\right) \left(\frac{1}{p} + \frac{1}{q}\right) \left(\frac{p}{q}\right)^\ell \sum_{j=1}^{\ell} j \left(\frac{q}{p}\right)^j.$$

This dwell time approximates those from the simulations best when $E_a$ is large and qualitatively matches them for small $E_a$. We can treat the cases depicted in Figs. S3D-F as repeated cycles marked by when ribosome and RNAP periodically meet each other. Therefore, in the large-$L$ limit, the effective velocities are approximately equal: $\overline{V}_{\text{rib}} = \overline{V}_{\text{RNAP}} \equiv \overline{V}$.

**Analytic approximation of the effective velocity.** To calculate the overall effective velocity, we evaluate the effective velocity in each of the two metastates. For the metastate $d > \ell$, if $p < q$, then the ribosome is always processive and the effective velocity $v_0 = p$ is directly given by $p$. When $p > q$, the RNAP is also processive in this state, and the speed $v_0 = q$ is dependent on the slower RNAP. In conclusion, $v_0 = \min\{p, q\}$. In metastate $d \le \ell$, the mean/effective velocity $\overline{V}$ is an weighted average of the speed of the processive state defined in Eq. S20 with weight $\sim k_+^*/(k_+^* + k_-)$ and the speed 0 of the paused state. with weight $\sim k_-/(k_+^* + k_-)$:

$$v_1 \approx q \left[\frac{(q/p)^\ell - 1}{(q/p)^{\ell+1} - 1}\right] \frac{k_+^*}{k_+^* + k_-}. \tag{S21}$$

The overall effective velocity is then given by Eq. 17:

$$\overline{V} \approx \frac{T_0}{T_0 + T_1} v_0 + \frac{T_1}{T_0 + T_1} v_1.$$

Note that $v_0 \ge v_1$. For sufficiently large $q$ and $\ell$, the coefficient $\left[\frac{(q/p)^\ell - 1}{(q/p)^{\ell+1} - 1}\right] \sim p/q$ and $\overline{V} \approx pk_+^*/(k_+^* + k_-)$ as expected. Since $k_+^* \ge k_+$, the effective velocity satisfy the lower bounds given in Eq. 18.

**Analytic approximation of the coupling coefficient $C$.** A way to directly compute the coupling coefficient is suggested by the fact that the ribosome and RNAP are only coupled for a fraction of time $k_a/(k_a + k_d)$ in metastate $d \le \ell$, as indicated by Eq. 15:

$$C \approx \frac{k_a}{k_a + k_d} \frac{T_1}{T_1 + T_0}.$$

**Analytic approximation of the protected time fraction $F_T$.** To approximate $F_T$, we assume that $\ell < \ell_p$. Therefore, $d > \ell_p$ occurs only in metastate $d > \ell$. Recall that we have separated $T_0$ into two components, the iid trials and the compensation for drift. We assume for simplicity that during the compensation process, $d > \ell_p$ always holds. We then evaluate the probability and fraction of time of exposure during the iid trials.

The largest distance $d_{\max}$ during one of the iid trials is determined by the waiting time $\tau_- \sim \text{Exp}(k_-)$ of RNAP pausing. Then, $d_{\max} \approx (q-p)\tau_-$. In this calculation, we treat the movement $(q-p)$ as a deterministic process while the main stochasticity arises from an exponentially distributed $\tau_-$. Before the RNAP pauses again, the distance $d$ grows linearly with speed $(q-p)t$. After the RNAP pauses, the distance $d$ shrinks with speed $pt$. Therefore, the total time of exposure is simply $q/p$ times the exposure time before RNAP pausing (analogous to "$\tau_{\text{uncoupled}}$" in Fig. S2 with $\ell \to \ell_p$). Since $(\ell_p - \ell)/(q-p)$ is an estimate

of the time for $d$ to reach $\ell_p$, we can evaluate the expectation $\mathbb{E}[\max\{\tau_- - \frac{\ell_p-\ell}{q-p}, 0\}]$ by using the memoryless property of exponential distributions

$$\mathbb{E}\left[\max\left\{\tau_- - \frac{\ell_p-\ell}{q-p}, 0\right\}\right] = \frac{1}{k_-}\mathbb{P}\left(\tau_- > \frac{\ell_p-\ell}{q-p}\right) = \frac{e^{-\frac{k_-}{q-p}(\ell_p-\ell)}}{k_-} \tag{S22}$$

Consequently, an approximation to the protected time fraction is given by Eq. 16:

$$F_T \approx \frac{T_1}{T_1+T_0} + \frac{\frac{q}{pk_-} + \left(\frac{1}{k_-}+\frac{1}{k_+}\right)\frac{(q-p)k_+}{pk_-}}{T_1+T_0}\left[1-\mathbb{P}\left(\tau_- > \frac{\ell_p-\ell}{q-p}\right)\right] = \frac{T_1}{T_1+T_0} + \frac{\frac{q}{pk_-} + \left(\frac{1}{k_-}+\frac{1}{k_+}\right)\frac{(q-p)k_+}{pk_-}}{T_0+T_1}\left(1-e^{-\frac{k_-}{q-p}(\ell_p-\ell)}\right)$$

## S5 Variability of the protected-time fraction $F_T$.

Fig. 3E plotted only the expected protected fraction. Since $F_T$ was generated via the full stochastic simulation, the variability of $F_T$ is also of interest. In Fig. S5, we plot the standard deviation $\sigma[F_T]$ versus simulated values of $F_T$ to show that it agrees qualitatively well with $\sqrt{\mathbb{E}[F_T](1-\mathbb{E}[F_T])}$.

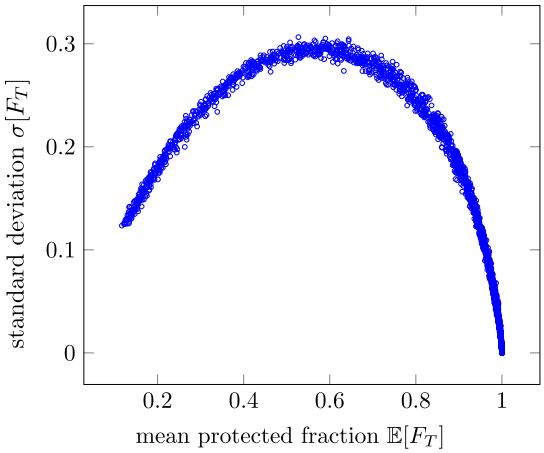


Figure S5: Standard deviation $\sigma[F_T]$ as a function of $\mathbb{E}[F_T]$ computed using different values of $(p, q)$. All other parameter values are those used in Fig. 3E.

## S6 Effects of interaction length $\ell$.

The interaction length $\ell$ is one factor that influences coupling-induced slowdown, as indicated by Eq. S21. The interaction length is not a significant contributing factor to slowdown because the factor $\left[\frac{(q/p)^\ell-1}{(q/p)^{\ell+1}-1}\right]$ is already $\sim 1$ when $\ell \sim 5$. This factor is small only when $\ell \approx 0$. Since $\ell$ takes on integer values this slowdown factor never really becomes very small. On the other hand, the interaction length $\ell$ also dictates the distribution of $d$ conditioned on $a = 1$. For example, if $\ell/p \gg k_-$, then the most probable distance between ribosome and RNAP will be $d = \ell$.

We have found an interesting "bifurcation" in effective velocity and mean protected times when the interaction distance $\ell > \ell_p = 27$ codons, the mRNA footprint length of a transcription terminator such as Rho. If $\ell < \ell_p$, protection by the ribosome can be thought of as being purely due to steric exclusion effects; once $d > \ell_p$, protection is lost. However, if $\ell > \ell_p$ one can consider a "binding-based" protection that requires either $d \le \ell_p$ *or* $a = 1$ for protection. In this case, even if $\ell > d > \ell_p$, there can be protection due to binding-mediated conformational shielding of the intervening mRNA that makes it inaccessible to termination factors. The different criteria for protection lead to drastically different levels of protection provided by the ribosome, as shown in Fig. S6.

## S7 Analysis of LacZ completion assays

In this section, we provide additional analysis and interpretation of the measurements obtained from LacZ assays. In these experiments, the completion times of RNAP and ribosome are measured separately. Thus, once can obtain only the density

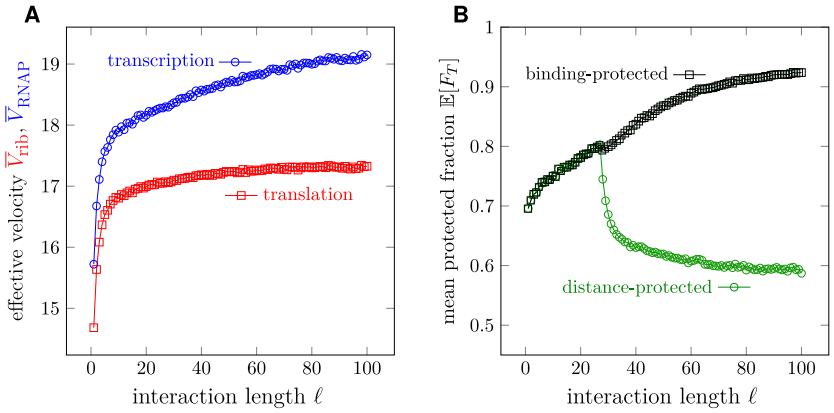


Figure S6: Functional consequences of varying interaction length $\ell$. Unspecified parameters are the same as those used in Fig. 3. (A) Effective velocities as a function of $\ell$. Note the sharp drop when $\ell \to 0$. (B) Bifurcation of $\mathbb{E}[F_T]$ as a function of $\ell$ due to different definitions of protection. Other parameters are the same as those used in the Fig. 3. When $\ell < \ell_{\rm p} = 27$ codons, the two definitions of $F_T$ agree. When $\ell > \ell_{\rm p}$, the $\mathbb{E}[F_T]$ based purely distance is drastically lower as $\ell$ increases.

of the times $T_{\rm RNAP}$ and of the times $T_{\rm rib}$, but not the joint density of both times or the density of the delay $\Delta T = T_{\rm rib} - T_{\rm RNAP}$. These two types of measurements provide signals $S_{\rm mRNA}(t)$ and $S_{\rm prot}(t)$ that are proportional to amount of mRNA and protein generated by a collection of cells up to time $t$, respectively.

In the time-of-flight experiments, assume the LacZ mRNA signal from each cell is $s_{\rm mRNA}$ is described by

$$s_{\rm mRNA}(t) = \begin{cases} 0 & \text{if } t < T_{\rm RNAP} \\ k(t - T_{\rm RNAP}) & \text{if } t \geq T_{\rm RNAP}, \end{cases} \tag{S23}$$

where we have neglected the relatively slow mRNA degradation and $k$ is the single-cell rate of mRNA production, an unknown parameter to be inferred by fitting to data. The leading RNAP completion time $T_{\rm RNAP}$ can be in principle experimentally measured by linearly extrapolating the single-cell mRNA signal in the long-time limit $t \geq T_{\rm RNAP}$.

Assume a collection of $N \gg 1$ identical independent cells in an experimental assay. From the underlying stochastic TTC process in each cell $1 \leq i \leq N$, the realizations $T_{{\rm RNAP},i}$ of RNAP completion times represent $N$ independent samples over the probability density $\rho(T_{\rm RNAP})$. The observed total mRNA signal $S_{\rm mRNA}$ is the sum of the mRNA signals $s_{{\rm mRNA},i}$ from each cell $i$ in the culture. Therefore, the slope of $S_{\rm mRNA}$ at time $t$ is proportional to the fraction of cells in the culture with RNAP completion times $T_{\rm RNAP}$ less than $t$. In an ensemble experiment using a large number of cells, this fraction is approximately defines the probability $\mathbb{P}(T_{\rm RNAP} \leq t)$:

$$\frac{{\rm d}S_{\rm mRNA}(t)}{{\rm d}t} \approx K\mathbb{P}(T_{\rm RNAP} \leq t), \tag{S24}$$

where $K = Nk$ (assuming all cells have identical production rates) is the steady state mRNA production rate of the collection of cells. Since $\mathbb{P}(T_{\rm RNAP} \leq 0) = 0$ and $\mathbb{P}(T_{\rm RNAP} < \infty) = 1$, we can define the mean $\mathbb{E}[T_{\rm RNAP}] \equiv \int_0^\infty \rho(T_{\rm RNAP}){\rm d}T_{\rm RNAP}$.

Next, we considered three hypothetical probability densities of $T_{\rm RNAP}$; one with a single peak, one with two adjacent peaks, and one with two well-separated peaks, respectively. $T_{{\rm RNAP},i}$ were then sampled from these distributions and $s_{\rm mRNA}(t)$ for each cell was constructed using Eq. S23. Summing the single-cell signals, we find the total mRNA signal $S_{\rm mRNA}(t)$ associated with each of the three densities and plot them in Fig. S7A. The corresponding probability densities are shown in Fig. S7B. Fig. S7C shows the probability density $\rho(T_{\rm RNAP})$ (rescaled so that its maximum value is set to one) found by simulating our model for different values of ribosome translation rate $p$. The parameter values are those used in Fig. 5D, namely, $q = 30,\ k_+ = 0.3,\ k_- = 0.4, E_+ = 2,\ k_{\rm a} = 100,\ E_{\rm a} = 3,\ \ell = 4$, and $L = 335$. About $10^4$ trajectories were generated to construct Fig. S7C. Typically, the measured signal is fit at long times to a linear function $Kt - B$ to find $B$ and extrapolated to zero to find the experimental estimate $\hat{T}_{\rm RNAP} = B/K$. As shown by the vertical dashed lines in Figs. S7A and B, the extrapolated estimates $\hat{T}_{\rm RNAP}$ are very close to the mean values $\mathbb{E}[T_{\rm RNAP}]$) for all three densities.

Modeling the protein signal $S_{\rm prot}(t)$ is slightly more complicated. For mRNA production, the number of genes associated with the transcript is constant throughout the mRNA production process. However, the number of mRNA templates for protein synthesis increases in time. Since polypeptide synthesis is initiated once the first ribosome initiates, it can be approximated to start when the ribosome initiation site is produced, right after the initiation of the first RNAP, defined as the zero of time in the

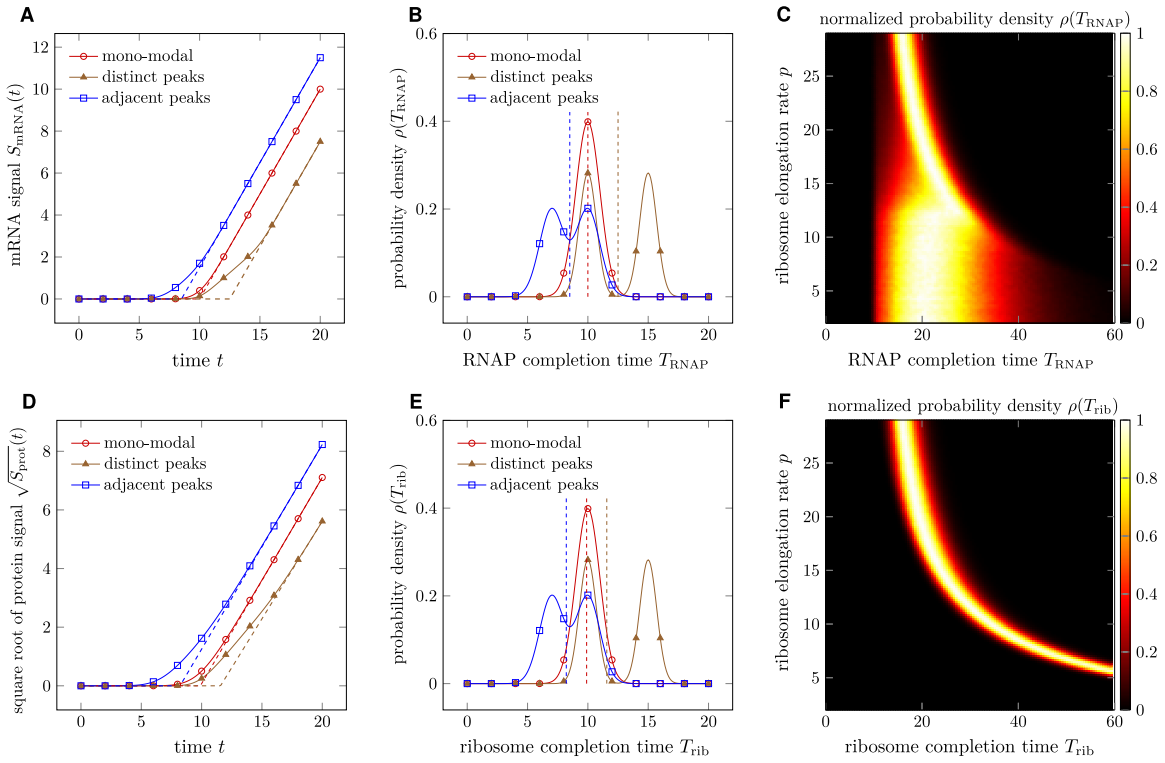


Figure S7: Simple examples of the ideal LacZ assay output signal $S(t)$ and the associated probability densities of the first completion time $T$. (A) The mRNA signal $S_{\mathrm{mRNA}}(t)$ produced by hypothetical distributions of $T_{\mathrm{RNAP}}$ with a single peak, two adjacent peaks, and two separated peaks, respectively using Eq. S24. (B) The underlying hypothetical distributions of $T_{\mathrm{RNAP}}$. (C) The rescaled heatmap shows the distribution of $T_{\mathrm{RNAP}}$ obtained from simulation of our model. (D) The square root of the output protein signal $\sqrt{S_{\mathrm{prot}}(t)}$ produced by hypothetical distributions of $T_{\mathrm{rib}}$ with a single peak, two adjacent peaks, and two separated peaks, respectively using Eq. S25. (E) The underlying hypothetical distributions of $T_{\mathrm{rib}}$. (F) The rescaled heatmap showing the distribution of $T_{\mathrm{rib}}$ obtained from simulation of our model. The parameters here and in (C) are those used to generate Fig. 5D. Dashed lines in (A,D) indicate the linear extrapolation of the observed curves. The intercepts of the linear fitted dashed lines are the experimental estimates for $\hat{T}_{\mathrm{RNAP}}$ and $\hat{T}_{\mathrm{rib}}$, which are also indicated by dashed vertical lines in (B,E).

experiments. Specific to each mRNA template $j$ is its associated first ribosome completion time $T_{\mathrm{rib},j}$. However, the template mRNA $j$ is only completed at a later time $\tau_j > 0$. At a given time $t$ after induction of gene expression, the production rate of protein is proportional to the integral from $\tau = 0$ to $\tau = t$ of the rate of template mRNA synthesis ($\approx K$) multiplied by the fraction of template mRNA that has entered the constant protein production phase $\mathbb{P}(T_{\mathrm{rib}} \leq t - \tau)$. Then, analogous to Eq. S24, we have the following expression for the protein signal:

$$\frac{\mathrm{d}S_{\mathrm{prot}}(t)}{\mathrm{d}t} \approx K \int_0^t \mathbb{P}(T_{\mathrm{rib}} \leq t - \tau)\mathrm{d}\tau = K \int_0^t \mathbb{P}(T_{\mathrm{rib}} \leq \tau)\mathrm{d}\tau. \tag{S25}$$

In the $t \to 0$ limit, $\mathbb{P}(T_{\mathrm{rib}} < t) \approx 0$ while in the $t \to \infty$ limit, $\mathbb{P}(T_{\mathrm{rib}} < t) \approx 1$. Therefore, the signal $S_{\mathrm{prot}} \approx 0$ initially but increases quadratically with time $t$ in the long-time limit. This quadratic dependence assumes no mRNA degradation and that ribosomes are not limited, and is consistent with experimental observations. Experimentally, $\hat{T}_{\mathrm{rib}}$ is estimated by linearly extrapolating, from long times, the square root of the protein signal $\sqrt{S_{\mathrm{prot}}(t)}$ to zero, as shown in Fig. S7D. For the different hypothetical $\rho(T_{\mathrm{rib}})$ shown in Fig. S7E, we used the same $\rho(T_{\mathrm{RNAP}})$ plotted in B. Again, the experimental estimates from extrapolation $\hat{T}_{\mathrm{rib}}$ are again close to the mean values $\mathbb{E}[T_{\mathrm{RNAP}}]$, although there is some deviation for the separated-peak density function. Fig. S7F plots the rescaled probability density $\rho(T_{\mathrm{rib}})$ found from simulating our model. The parameters are those used in Fig. 5D and Fig. S7C.

Limited by finite sampling frequency of experiments, signals can only be extrapolated, and the estimates $\hat{T}_{\mathrm{RNAP}}$ and $\hat{T}_{\mathrm{rib}}$ should be interpreted as the mean of their respective distributions. However, it is clear that if a higher temporal resolution can be achieved when measuring mRNA and protein signals, finer structure of the densities $\rho$ can in principle be inferred. By

separately plotting the simulated probability densities over the component times $T_{\mathrm{RNAP}}$ and $T_{\mathrm{rib}}$, we see that the bimodality in $\rho(\Delta T)$ near $p \approx 12$ codons/s as seen in Fig. 5D results mainly from the bimodality of $\rho(T_{\mathrm{RNAP}})$ (Fig. S7C) since $\rho(T_{\mathrm{rib}})$ is sharply peaked (Fig. S7F).

## S8 Supplementary Figures

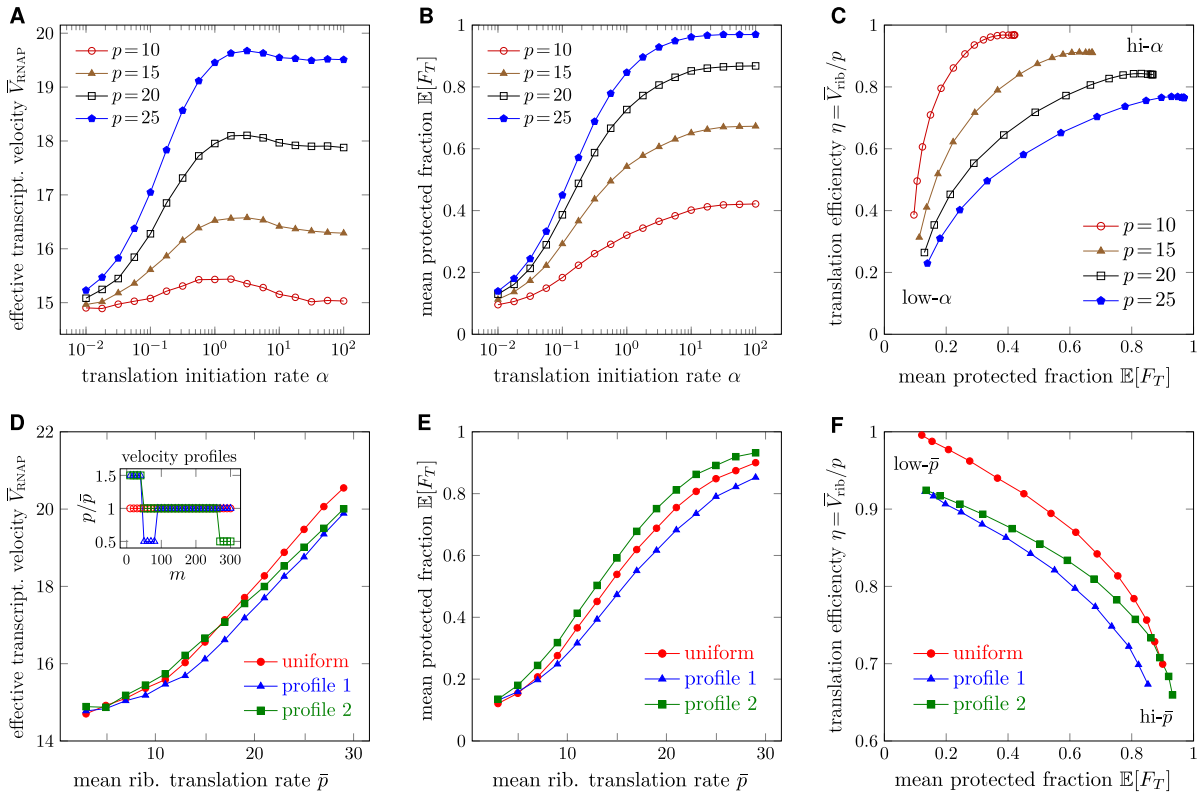


Figure S8: TTC and performance under genomic variability. Again, we use the standard set of fixed parameter values as in Figs. 4 and 5. (A) Effective transcription velocity $\overline{V}_{\mathrm{RNAP}}$ as a function of the translation-initiation rate $\alpha$. $\overline{V}_{\mathrm{RNAP}}$ initially increases as $\alpha$ is increased until about $\alpha \simeq 1$ s $^{-1}$, after which $\overline{V}_{\mathrm{RNAP}}$ decreases slightly as $\alpha$ is further increased. (B) Mean protected fraction $\mathbb{E}[F_T]$ as a function of the translation-initiation rate $\alpha$. (C) Efficiency *versus* protection fraction as $\alpha$ is varied. Larger $\alpha$ contributes to both efficiency and protection. As $\alpha$ is increased, the system spends more time protected. Since $\mathbb{E}[T_{\mathrm{rib}}]$ includes the ribosome initiation time, it decreases as $\alpha$ is increased, leading to an increased $\overline{V}_{\mathrm{rib}}$ and $\eta$. (D) and (E) $\overline{V}_{\mathrm{RNAP}}$ and $\mathbb{E}[F_T]$ as a function of the mean $\bar{p}$ under three different translocation rate profiles $p_m$. (F) The $\eta$-$\mathbb{E}[F_T]$ trade-off plot for three different profiles as the mean value $\bar{p}$ is varied. The inset in (D) illustrates the three translation-rate profiles. The overall performance of profile 1 suffers because of the slowdown following the initial fast translation. For $\bar{p} \leq 15$ codons/s, profile 2 has a higher $\overline{V}_{\mathrm{RNAP}}$ compared with the uniform profile. When $p \geq 15$ codons/s, the uniform profile still has a higher $\overline{V}_{\mathrm{RNAP}}$. For all values of $p$, profile 2 has a higher $F_T$ than the uniform profile because of its higher initial speed.

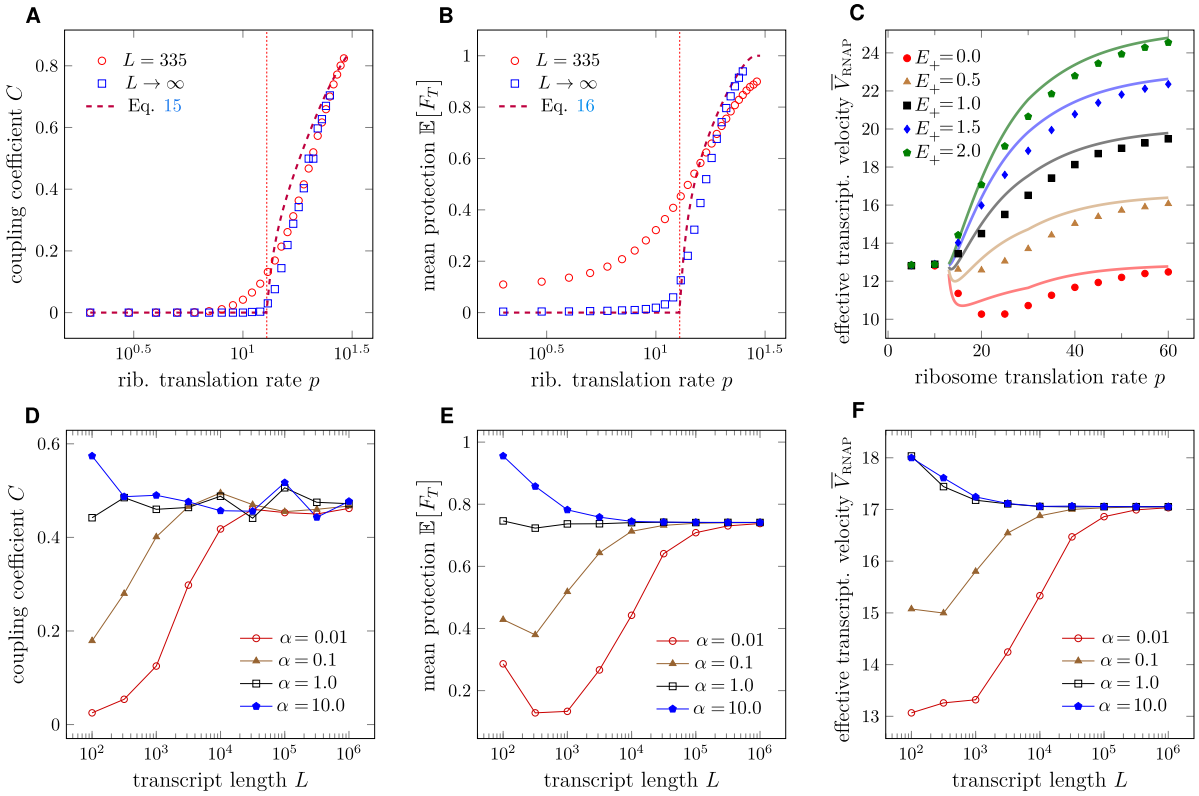


Figure S9: Validity of approximation formulae in the $L \to \infty$ limit and the interplay between translation initiation rate $\alpha$ and transcript length $L$. Here, unspecified parameters assume the same value as in Fig. 3. (A) Comparison of coupling coefficient $C$ of different transcript lengths $L$ as a function of $p$ when $q = 30$ codons/s. We take $L = 10^6$ codons as the surrogate for $L \to \infty$. In general, $L = 335$ and $L \to \infty$ generate approximately similar coupling coefficients $C$; however, the kink at $p = \bar{q}$ (marked by red dashed vertical lines) for $L \to \infty$ is better captured by Eq. 15. (B) Comparison of mean fraction of protected time $\mathbb{E}[F_T]$ as a function of ribosome translation rate $p$ with different $L$ when $q = 30$ codons/s. We also take $L = 10^6$ codons as the surrogate for $L \to \infty$. The difference between $L = 335$ and $L \to \infty$ is significant, and Eq. 16 agrees better with the $L \to \infty$ simulation results. (C) Comparison of the effective transcription velocity $\overline{V}_{\mathrm{RNAP}}$ for different $p$ and $E_+$ in an $L = 10^4$ system. Other parameters are the same as those used in Fig. 4B. (D) Coupling coefficient $C$ as functions of $L$ and translation initiation rate $\alpha$. (E) Mean fraction of protected time $\mathbb{E}[F_T]$ as a function of $L$ and $\alpha$. (F) Effective transcription velocity $\overline{V}_{\mathrm{RNAP}}$ as a function of $L$ and $\alpha$.